Unexpected harvesting-induced evolution of collective behavior in a fish

Valerio Sbragaglia[a,b,1,2], **Pascal P. Klamser**[c,d,1], **Pawel Romanczuk**[c,d,3], **and Robert Arlinghaus**[a,e]

[a]Department of Biology and Ecology of Fishes, Leibniz-Institute of Freshwater Ecology and Inland Fisheries, Müggelseedamm 310, 12587 Berlin, Germany
[b]Department of Marine Renewable Resources, Marine Science Institute (ICM-CSIC), Barcelona, Spain
[c]Department of Biology, Institute for Theoretical Biology, Humboldt-Universität zu Berlin, 10115 Berlin, Germany
[d]Bernstein Center for Computational Neuroscience, 10115 Berlin, Germany
[e]Division of Integrative Fisheries Management, Department of Crop and Animal Sciences, Faculty of Life Science, Humboldt-Universität zu Berlin, Invalidenstrasse 42, 10115 Berlin, Germany

Many fisheries around the globe selectively capture large individuals with potential evolutionary consequences for exploited populations. Fisheries-induced evolution in response to intensive and size-selective harvesting may trigger individual behavioral changes, which in turn may affect collective behavior. Studying the cause-and-effect of intensive and size-selective harvesting is challenging in the wild, but insights can be gathered through experimental evolution in the laboratory. Previous results from a multi-generation harvest selection experiment with zebrafish (*Danio rerio*) as a model species demonstrated that large size-selective harvesting typical of global fisheries decreased collective risk-taking behavior, while the opposite was observed for small size-selective harvesting. Here, we investigate a possible link between collective risk-taking behavior and shoal cohesion. Surprisingly, the large-harvested line (i.e., the treatment characterized by a decrease of risk-taking) showed a decrease of shoal cohesion, while the opposite was observed for the small-harvested line. We propose a mechanistic explanation for this counter-intuitive finding through an increased vigilance of individuals of the large-harvested line towards environmental cues at the expense of attention paid to social cues (and vice versa for individuals of the small-harvested line). Agent-based model simulations further revealed that the changes of collective behavior in response to large size-selective harvesting might be adaptive under fishing scenarios by decreasing exploitation rate. By contrast, the same collective behavior favored by large size-selective harvesting might be maladaptive in the presence of natural predation and increase natural mortality. The harvesting-induced changes we documented may slowly, but steadily erode the natural fitness benefits offered by shoaling in many species targeted by global fisheries. Fisheries-induced evolution of collective behavior may negatively affect population recovery and catchability with consequences for human well-being.

boldness | **cohesion** | **vigilance** | **catchability** | **maladaptive** | **fishing** |

[1] V.S. and P.P.K. contributed equally to this work.

Correspondence:

[2]experimental data: valeriosbra@gmail.com

[3]models and simulations: pawel.romanczuk@hu-berlin.de

Contributions:

V.S. and R.A. designed the experiments; V.S. performed the experiments, the statistical test and analysed part of the experimental data. P.P.K. and P.R. developed the model. P.P.K. ran the simulations and analyzed part of the experimental data. V.S., P.P.K., P.R. and R.A. interpreted the data. V.S., P.P.K, P.R. and R.A. wrote the manuscript.

Introduction

Human harvesting of wild animals may trigger evolutionary changes in exploited populations (1, 2). Intensive and size-selective fishing can evolutionary alter life-history as well as physiological and behavioral traits (3–6). Fisheries-induced evolution of both life history and behavior may ultimate decrease catchability and recovery and is thus relevant from a fisheries-management perspective (7).

The mechanisms governing fisheries-induced evolution of individual behavior are poorly understood (1, 8). Moreover the role of evolutionary changes of individual behaviour in driving collective behavior is largely unexplored in a fisheries-induced evolutionary context. Collective behavior characterizes many fish species, including those of high relevance for global fisheries (e.g. small pelagics such as anchoveta, *Engraulis ringens*, and Atlantic herring, *Clupea harengus*). In fact, 13 out of the 25 most fished species in the world are strongly shoaling fish that account for about a quarter of total fisheries landings (9). Therefore, fisheries-induced evolution of collective behavior could have implications for the management of many fish species that sustain global fisheries.

Fish shoaling behavior is a key driver of the capture process, e.g., in seining or trawling (10–12). Shoaling also has strong natural adaptive value by reducing predation risk and in some cases increasing foraging efficiency (13–15). The emergence of collective behavior in fish and other animals can be explained by simple interactions rules among individuals that are influenced by their respective neighbours (16–18). Major group-level behavioural transitions can be triggered by minor changes in social interactions at the individual level (19). Therefore, fisheries-induced evolution could affect collective outputs such as shoaling by changing individual behavioral traits (e.g. risk taking behavior; (20)) that are involved in the interactions rules that drive group behavior.

Large size-selective harvesting, where larger fish have a higher mortality risk than smaller ones, is a typical selectivity pattern in fisheries. A recent theoretical model predicts that size-selective harvesting may favor either bold phenotypes when the size-selectivity is not very pronounced or shy phenotypes when the size-selectivity is very pronounced and only very large, adult fishes are selectively harvested (3). Individual changes in behavior may in turn also affect collective phenotypes, such as shoaling. Several mechanisms could shape how fisheries-induced evolution of individual pheno-

DRAFT

types may affect collective behavior. For example, heterogeneity of individual behavior can play an important role in driving collective behavioral outputs such as shoal cohesion (21), as shown in qingbo, *Spinibarbus sinensis*, where shoals composed of either exclusively shy or bold individuals were less cohesive than shoals formed by individuals with a diversity of boldness levels (22). Also slow individual swimming speed increases shoal cohesion as shown for different fish species (22–24). In addition, shoal cohesion may be affected by a trade-off between vigilance (i.e. the frequency of environmental scans), and the use of social cues within a shoal. Vigilance can be affected by group size (25–27) or social behavior (e.g. territorial aggression (28)). How vigilance influences cohesion is to our knowledge largely unexplored in general and in a size-selective mortality context. Yet, shoals predominantly composed of individuals with reduced risk-taking behavior – i.e. shy individuals, which is an adaption predicted in fisheries-induced evolution under large size-selective harvesting (3, 20) - might be more vigilant (29, 30) at the expense of paying less attention to their conspecifics, in turn reducing shoal cohesion. Considering that individual risk-taking behavior is expected to systematically shift with fisheries-induced evolution (20), important effects on shoaling behavior are thus likely (31), but a mechanistic explanation is still missing.

Mechanistically, the swimming behavior of many fish can be characterized by the tail beat frequency (32), which allows to split the trajectories in burst phases (i.e., speed increases) followed by coast phases (33). Zebrafish (*Danio rerio*) exhibit a burst-coast-type swimming behavior that can be quantified from tracking data (33). Different burst rates lead to differences in group cohesion and speed (34). However, previous burst-coast models considered only social cues (33, 34), neglecting the importance of environmental cues, which may trigger burst responses of individual fish in a group. A full characterization of the individual-level mechanisms governing collective behavior should take into account all possible processes affecting individual behavior (in particular those related to risk perception) and the emerging output at the group level. In this context, exploring systematic variation in individual perception of, and response to, environmental cues as opposed to just social cues, is essential for developing a holistic understanding of how changes in individual risk perception may affect collective behavior under size-selective mortality from a mechanistic perspective.

We take advantage of a long-term harvesting experiment of zebrafish as a model shoaling species. Experimental lines were subjected to five generations of opposing size-selective harvesting (6): large-harvested line (larger individuals harvested, the typical case in most fisheries), small-harvested line (smaller individuals harvested, a possible case in fisheries managed with a maximum-size limit or where dome-shaped selectivity is prevalent) and random-harvested line (control). Previous results revealed substantial changes in life history, body size, gene expression, allele frequencies as well as individual and collective behavioral traits (6, 31, 35–38). In particular, the large-harvested line showed a decreased collective risk-taking behavior, while the small-harvested line increased it with respect to control (36). It is an open question to be addressed in this study whether and how such changes in collective risk-taking behavior affect shoaling behavior.

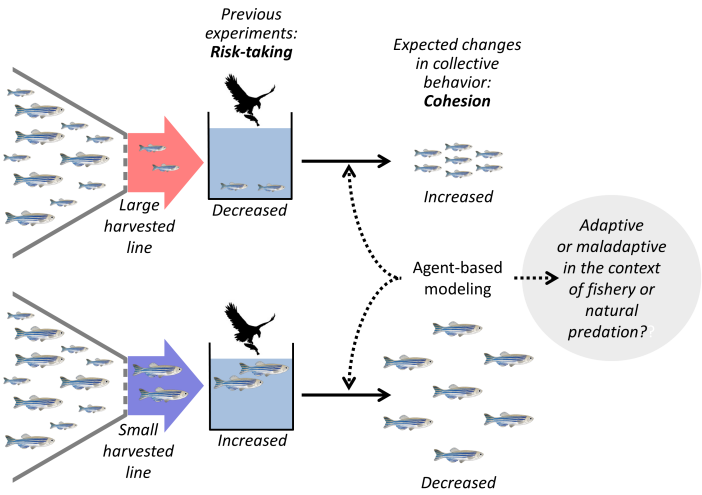

Fig. 1. The conceptual framework used in our study. Previous experiments showed that size-selective harvesting triggered changes in collective risk-taking by decreasing it in the large-size selective line and increasing it in the small-harvested line compared to controls (36). The solid arrows represent the experimental hypothesis tested in our study according to classic theory in collective behavior (13). Note that changes in shoal cohesion are expected relative to controls in both size-selected lines. Next, we calibrated an agent-based model to mechanistically understand the process driving the resulting collective phenomena (dotted arrows). Finally, we used the model to simulate different fishing and natural predator scenarios to explore adaptive or maladaptive value of evolutionary changes in collective behavior. Zebrafish pic source: https://commons.wikimedia.org; Bird pic source: https://www.piqsels.com

Classic theory related to group living animals predict that a decrease of risk-taking behavior should result in individuals forming more cohesive shoals to reduce their probability of predation mortality (13, 39). Therefore, we predicted that the decrease of collective risk-taking behavior observed in the large-harvested line would be linked to an increase of shoal cohesion (Fig. 1; and vice versa for the small-harvested line). Next, to fully understand the mechanistic process driving the possible differences in shoal cohesion among the selection lines, we developed an agent-based model that related individual-level traits (e.g., swimming speed and burst rate using environmental vs. social cues) to group-level emergent properties (Fig. 1). To that end, we used high resolution tracking of individual fish within groups to calibrate the burst-coast-agent-based model. Lastly, we used the model to simulate the collective behavior of the selection lines in the presence of a natural predator or fishing gear to explore adaptive or possible maladaptive outcomes of fisheries-induced evolution of collective behavior in natural and human-shaped eco-evolutionary contexts (Fig. 1). In summary, our paper presents novel experimental data on the possible evolutionary changes in shoal cohesion as well as theory to mechanistically explain our findings. The results are synthesized through simulations to provide predictions in terms of possible shoaling-mediated outcomes in exploited populations exposed to both fishing gear and natural predators.

DRAFT

Results

A. Shoaling behavior. In group-level experiments we found a significant effect of the selection lines on both mean nearest-neighbor distance ($\chi^2_{(2)} = 7.8$; $p < 0.05$; Fig. 2A) and mean inter-individual distance ($\chi^2_{(2)} = 8.8$; $p < 0.05$; inset in Fig. 2A). In particular, the large- and small-harvested lines formed less and more cohesive shoals than controls, respectively (Fig. 2A); the same pattern was observed for the nearest-neighbor distance (Fig. 2A). This result was counter-intuitive and at odds with our study hypothesis because we initially (Fig. 1) had assumed that the less risk-taking behavior of the large-harvested individuals would have triggered more cohesive shoals than controls. We found the opposite. Our results were further supported by a negative correlation (R = 0.26; $F_{(1,28)}$= 9.8; p < 0.01) between mean nearest-neighbor distance and the previously documented risk-taking behavior (Fig. 2B; note that in this study we used the same groups of fish previously used to test risk-taking behavior, see methods for more details). Furthermore, the inter-individual distance and the nearest-neighbor distance also showed a strong positive correlation (R = 0.87; $F_{(1,28)}$= 193.4; p < 0.001), which means that the change in inter-individual distance was not related to a split of the main group into multiple subgroups.

B. Fish body size and individual behavior in the shoal. As expected, the body size at age of the experimental fish varied significantly among the selection lines ($\chi^2_{(2)} = 28.3$; $p < 0.001$; Fig. 2C).

We individually tracked fish behavior during shoaling (see methods for more details). The individual burst rate during collective movement was significantly ($\chi^2_{(2)} = 44.6$; $p < 0.001$) different among selection lines. Specifically, the small-, but not the large-harvested line, bursted less frequently than controls (Fig. 2D). Furthermore, the individual swimming speed was significantly ($\chi^2_{(2)} = 47.8$; $p < 0.001$) different among selection lines. Again, the small-, but not the large-harvested line, showed a slower swimming speed than controls (Fig. 2E). Note that the burst rate showed a positive correlation with the swimming speed (R = 0.51; $F_{(1,142)}$= 146.5; p < 0.001; Fig. 2F), which suggests that differences in burst rate was the main cause of variation in swimming speed.

To control possible confounding effects of body size on the effects of size-selective harvesting on behavior (see methods for more details) we composed a subsample of the dataset with size-matched individuals without significant ($\chi^2_{(2)} = 1.1$; $p = 0.592$) differences in body length among the lines (Fig. 2C). The above mentioned differences in speed and burst rate among the selection lines were still significant for both burst rate ($\chi^2_{(2)} = 34.1$; $p < 0.001$; Fig. 2D) and speed ($\chi^2_{(2)} = 32.6$; $p < 0.001$; Fig. 2E) when the subsample of size-matched individuals was used in the analyses. Moreover, body size did not relate to burst rate ($\chi^2_{(2)} = 0.03$; $p = 0.858$) and swimming speed ($\chi^2_{(2)} = 0.4$; $p = 0.519$).

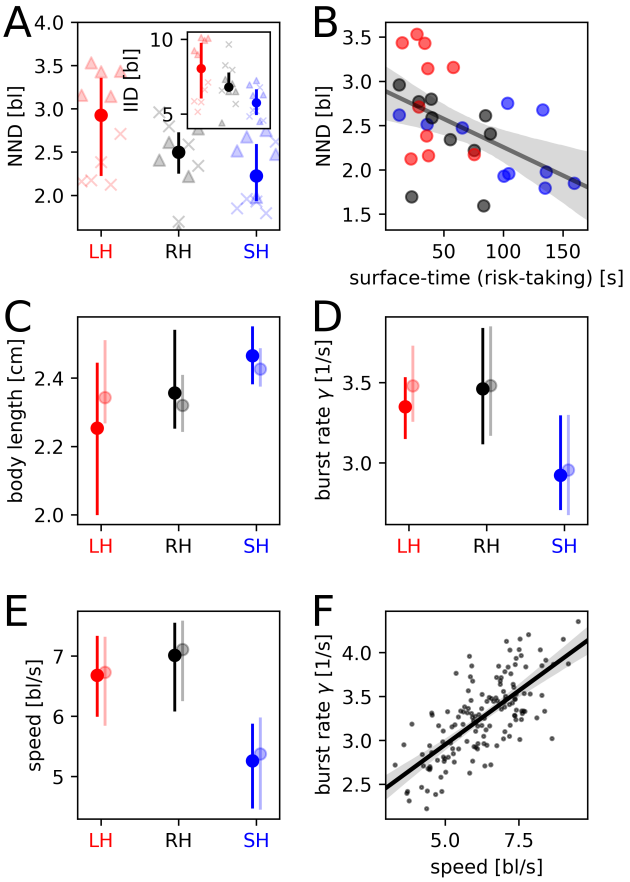

Fig. 2. Group level results for mean group nearest-neighbor distance (expressed in body length; **A**) and inter-individual distance (expressed in body length; inset **A**) together with the correlation between mean group nearest-neighbor distance and previously documented risk-taking behavior (i.e. time spent feeding at the surface, **B**; see (36) for more details; note that in this study we used the same groups of fish previously used to test risk-taking behavior, see methods for more details). Individual level results for body size (**C**), burst rate (**D**), and speed (expressed in body length per second; **E**) according to high resolution tracking (30 frames per second), as well as the correlation between burst rate and speed (**F**). The selection lines are indicated by different color (red=LH: large-harvested; black=RH: random-harvested; blue=SH: small-harvested). Bold colors (**C-E**) refers to the entire data set (N = 48), while transparent colors refers to the subsample of size-matched individuals (N = LH: 24; RH: 36; SH: 40). Points represent the median and vertical lines represent the first (25th percentile) and third (75th percentile) quartiles. Transparent triangles and crosses (**A**) correspond to raw data of the two different replicates.

C. Mechanistically linking micro-level interactions among individuals with macro-level collective outcomes. To unravel the mechanistic underpinning of our results, we implemented a burst-coast-agent-based model. An important aspect of the model is that each individual burst event (Fig. 3A) represents either a response to a random environmental cue (with probability P_{env}) or to a social cue (with probability $P_{soc} = 1 - P_{env}$). Thus, the vigilance is defined as the rate of bursts based on environmental cues, i.e. it is the product of burst rate γ and probability to follow an environmental cue P_{env}: $\gamma_{env} = \gamma P_{env}$. We propose that the decrease in risk-taking behavior of the large-harvested line triggers an increase in vigilance (29, 30), which causes a decrease in cohesion because of the random nature of false threat cues and the trade-off between vigilance and social attention.

To test this mechanistic explanation, the vigilance (as defined above) was calibrated, via the probability P_{env}, such that the simulations matched the experimental values of the nearest-neighbour distance (Fig. 2A) and the individual swimming speed (inset in Fig. 2C) for each selection line. The burst rate γ and duration t_b were set according to empirical data (Figure S.1). We assumed the remaining model parameters to be identical between the different selection lines, in line with empirical data (Tables S.2, S.3). The calibration of the burst-coast model suggested that our experimental measures were best reproduced by the model if the large-harvested line was more vigilant (Fig. 3B), and the small-harvested line less vigilant than the control (Fig. 3B). We thus conclude that differences in vigilance, which combines the differences in burst rate and probability to follow environmental cues, provide a putative mechanistic explanation for the observed differences in average individual swimming speed and nearest neighbor distance among the selection lines. Importantly, the differences in vigilance were also in qualitative agreement with the experimentally observed collective risk-taking behavior because the large-harvested line was found to be less risk-taking (i.e., shyer) than the control, while the opposite was observed for the small-harvested line ((36); see also Fig. 1).

D. Adaptive value of altered collective behaviour. We used the above-derived agent-based model representations of the three selection lines to finally investigate whether the size-selective harvest could impact the ability of the shoals to evade a natural predator and different fishing gear (see methods and SI for details). The mean exploitation rate (i.e. number of fish killed or captured per time) was computed in three different scenarios: (i) natural predation, including the possibility of a confusion effect (40), by a single mobile predator following the closest shoaling fish (Fig. 4A); (ii) fishing by a single agent without information about the position of the shoal (random search, similar to Fig. 4A; e.g., a fisher on a boat without an echo sounder); (iii) fishing by multiple aligned agents moving on a straight line towards the center of mass of the shoal (Fig. 4B; e.g., commercial trawling informed on the position of the shoal). Passive (e.g., a trap or hook-and-line sets) and active (e.g., seining or trawling) fishing gears were simulated by varying the speed of the fishing

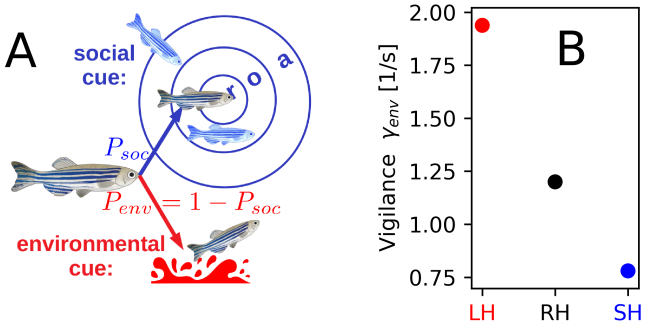

Fig. 3. (**A**) Schematic model description showing that at each burst an individual can follow with probability P_{soc} social cues (i.e. behaves according to a three-zone model: r=repulsion-, o=orientation-, a=attraction-zone) or with probability $P_{env} = 1 - P_{soc}$ environmental cues. (**B**) Optimization results of the environmental burst rate $\gamma_{env} = \gamma P_{env}$ for fitting the burst-coast model to experimental data. The selection lines differed, next to the fitted probability to follow social cues P_{soc}, in their burst rate γ and duration t_b which were estimated from experimental data. The selection lines are indicated by different colors (red=LH: large-harvested; black=RH: random-harvested; blue=SH: small-harvested). No error bars exist for the optimization. See methods for the robustness of the optimization results. Zebrafish pic source: https://commons.wikimedia.org .

agents in the simulated scenarios. Fishing agents were able to capture a fish if it was closer than $r_{capture}$ thereby creating an encounter-based capture mechanism typical of many fisheries (41, 42), while the natural predator's capture was also influenced by the number of shoaling fish in its vicinity (i.e. confusion effect, see methods). Our simulation thus captured a large variety of cases where fish mortality is imposed by fishing gear or natural predation.

The natural predator (Fig. 4C) exploited the large-harvested line faster than the controls; while the opposite was observed for the small-harvested line (Fig. 4C). By contrast, in all fishing scenarios (Fig. 4D, E), the fishing agents exploited the large-harvested line at a slower (i.e., less efficient) rate than the controls, and again the opposite was observed for the small-harvested line (Fig. 4D, E). Results are shown as relative standardized exploitation rate with respect to the controls (non-standardized values are shown in Figure S.3). Both size-selected lines revealed significant ($p < 0.001$) differences in exploitation rate with respect to the control except for two cases in the natural predator scenario where the small-harvested line did not show significant differences relative to the control (Fig. 4C; Table S.1). The difference between natural predation and the fishing scenarios vanished when the confusion effect was disabled in the model (Fig. S.3B) indicating that the differences in group cohesion among the selection lines caused opposing patterns in avoiding natural predator and fishing agents. Note that the same results were obtained if the distance between fish and fishers/predator was used as alternative measure to the exploitation rate (Fig. S.3I-P). To summarize, the simulation results suggested that the collective behavioural traits of the large-harvested line may increase survival in a fisheries context, but at the same time may increase mortality in a natural predation context, while the opposite was observed for the small-harvested line. The evolutionary changes in shoaling thus created fundamental trade-offs in exploited populations suggesting decreased mortality by fishing gear at the expense

DRAFT

of increased mortality by natural predation.

Discussion

We showed that size-selective harvesting fostered changes in shoal cohesion in the opposite direction to what was expected considering classic theory and the previously documented changes in collective risk-taking behavior ((36); Fig. 1). Our experimental hypothesis was rejected because a decrease in collective risk-taking behavior was not linked to an increase in shoal cohesion in the large-harvested line (and vice versa for the small-harvested line). By using an agent-based model we detected a possible explanation: by reducing risk-taking behavior, individuals of the large-harvested line were more vigilant, by frequently reacting to possibly threatening environmental cues, which in turn reduced their attention to social cues. Both effects reduced their shoal cohesion in contrast to what we had hypothesized. Importantly, we demonstrated the exactly opposite change in the small-harvested line, thereby showcasing that our results represented clean experimental outcomes that can be linked to the impact of size-selective harvest on individual-level behavioral changes, which in turn affect emergent collective behavior.

The changes of shoal cohesion we documented may be interpreted in light of a behavioral-mediated resource acquisition mechanism that affected size-at-age as trait under selection (36, 43). Zebrafish can attain a higher food consumption rate when they are in small groups than alone (44). Therefore, the large size-selective harvest could have removed bolder individuals that fed in small groups because such behavior could have provided advantages in accessing food and hence increased size-at-age; this could have fostered the evolution of reduced shoal cohesion. However, when assaying individual sociability the large-harvested line was not found to differ from controls (31). Thus, it is unlikely that direct selection on individual sociability is an explanation for the reduced shoal cohesion that we documented here.

The burst-coast-agent-based model linked risk-taking behavior with shoal cohesion and further helped explaining the harvesting-induced changes in collective behavior by assuming the existence of a trade-off between social and environmental information in collective motion (45). Our model is similar to previous work in terms of splitting the movement of shoaling fish into an active and passive phase (18, 33, 34). However, it provides a novel perspective about collective movements of fish shoals by linking risk perception and movement decisions. In fact, most previous models of collective behavior only accounted for social information (18, 19, 34, 46, 47), while our model explicitly implements the trade-off between random environmental and social cues. The previous simulation studies which considered similar mechanisms (e.g., when moving agents directly react to a non-conspecific cue as a predator (48, 49) or a food-patch (50)) allowed the moving agents to access non-social information without a permanent cost, i.e. the trade-off only exists with a present environmental cue. In our model, the vigilance limits the general capacity to react to social cues and thus affects the individual behavior even in the absence of environmental cues. Another major difference to most existing models (18, 19, 23, 47) is that the individual speed is not a model parameter but emerges from the interplay of burst rate, strength, duration and the tendency to follow environmental cues. Especially, accounting for the possibility of individual burst being triggered by either social or environmental cues adds a novel, yet ecologically relevant behavioral dimension to our agent-based model.

The simulations of natural predation and harvest revealed that the collective behavioral changes of the large-harvested line are likely maladaptive under natural predation, but are adaptive in a fishing context (and vice versa for the small-harvested line). Specifically, in our simulations the increase in vigilance of the large-harvested line decreased vulnerability of shoals under a multitude of simulated fishing scenarios considering passive and active gear as well as single and multiple fishing agents. Fisheries-induced evolution of maladaptive collective behavioral traits (i.e. shoal cohesion) can have strong repercussions in many shoaling teleosts when attempting to reduce risk of natural predation (15). Our study suggests that intensive fishing mortality directed at the larger individuals of a population could shift the fitness optimum of shoaling behavior in the opposite direction of what natural selection would favor. Adaptive evolution under anthropogenic selection has been demonstrated to occur within few generations (1, 4, 6, 51–53), and could impede recovery of exploited population even after harvesting halted (54). Interestingly, our results agree with an early bioeconomic model about fisheries-induced evolution that assumed shoaling behavior as evolving trait governed by a single gene (55). Shoaling behavior was modelled by producing two possible binary values (shoaling or not shoaling) and modelling results indicated that suboptimal management strategies may results in the extinction of valuable behavior evolved under natural selection (shoaling). The authors explained the results assuming that not shoaling behavior is supposed to be optimal under fishing pressure as we showed in our study. Our study provides the first functional integration of individual behavior into mechanisms governing group dynamics in the context of fishing exploitation. Moreover, our work proposes a new mechanism that could increase the natural mortality associated with fisheries-induced evolution and thereby negatively affect recovery, even if harvesting halted.

Previous studies have shown that fisheries-induced evolution of life histories can substantially increase natural mortality (56, 57). Elevated and size-selective harvesting triggers the evolution of a fast life-history, characterized by early maturation and small size, elevated reproductive investment and reduced post-maturation growth (58). Natural mortality decreases with length in fishes (59); therefore a decrease in body size is linked to an increase in natural mortality. In addition, an increase in reproductive investment is associated to an increase in natural mortality due to the cost of spawning (56, 60). Moreover, elevated and unselective fishing mortality is expected to increase risk-taking behavior, which in turn increases natural mortality (56). Previous experimental results using the zebrafish selection lines indicated that

DRAFT

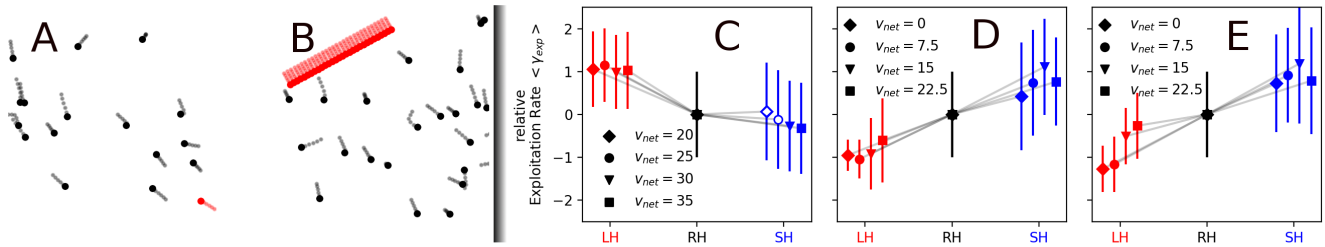

Fig. 4. Results of the "natural predator" (**A, C**), the "single-" (**A, D**) and the "multiple fishing agent" scenario (**B, E**). $N = 30$ shoaling fish were simulated in a box of size $L = 100\ cm$ with periodic boundary conditions. Their mean individual speed was about $\langle v \rangle \approx 15\ cm/s$. The predator moved with $v_{net} = [20,\ 25,\ ,30,\ 35]\ cm/s$ while the fishing agents with $v_{net} = [0,\ 7.5,\ 15,\ 22.5]\ cm/s$ indicated by star, circle, triangle and square marker, respectively. (**C, D, E**) Exploitation rates were reduced by the mean and divided by the standard deviation of the random-harvested line to standardize their values. Snapshots of a typical simulation are shown for the predator- and single-fishing-agent scenario (**A**) and for the multiple-fishing-agents scenario (**B**); the shoaling fish are represented in black and the predator and fishing agents in red. The colors red, black and blue of the marker correspond to the large- (LH), random- (RH) and small-harvested (SH) selection line respectively. The markers and error bars indicate the mean and standard deviation estimated from samples of 400 simulations. Empty symbols (**C**) represent not significant differences with respect to control (see Table S.1 for more details).

elevated mortality in combination with large size-selective harvest decreased collective risk-taking behavior (36), which agrees with recent theoretical work (3). Yet, while decreased risk-taking might reduce natural mortality, we propose that the decrease in shoal cohesion emerging from the evolution of decreased risk-taking behavior can be a further mechanism by which natural mortality increases in a fisheries-induced evolution context where large individuals are preferentially harvested. We therefore extended the framework presented by Jørgensen and Holt (56) for unselective fisheries harvest revealing an insofar unknown mechanism by which fisheries-induced evolution of individual behavioral trait (e.g. risk-taking behavior) through size-selection may drive collective outcomes that may be maladaptive under natural predation and elevate mortality in shoaling fishes. This is particularly important in an ecosystem context where trophic flow between predator and prey is controlled by a bottom-up mechanism mediated by prey behavior (61).

The size-selection treatments significantly affected both nearest-neighbor distance and inter-individual distance by accounting for the replicate of each selection line as a random effect in the statistical model (Table S.4). Although our approach is statistically rigorous, the two replicates within each of the two size-selection lines did not show comparable phenotypic responses in terms of nearest-neighbor distance and inter-individual distance (Fig. 2A). Indeed, when analyzing each replicate individually against the others selection lines we found that in both cases (large-harvested and small-harvested line) one of the two replicates was significant compared to controls while the other was not (Table S.4). We thus cannot exclude the potential for genetic drift or chance events in specific replicates having contributed to the phenotypic divergence in collective behavior among the selection lines. Other non-genetic factors could have contributed to the results such as small difference in the environment (e.g., slightly different biomass densities due to varying growth rates) with consequent effects on the resulting behavioral traits, as demonstrated for clonal fish (62). However, because the mixed effects statistical modeling (i.e., the line replicate as random effect) support opposing changes in collective behavior compared to control, we feel confident that the behavioral changes documented here were in response to the size-selection treatment rather than being caused by genetic drift. Indeed, recent results from a landmark study about experimental size-selective harvesting with Atlantic silversides (*Menidia menidia*) showed different responses of two replicates at the genomic level concluding that size selection caused consistent patterns of parallel divergence that cannot be expected by random drift (63). Similarly, quantitative genetics results about a similar experimental size-selective harvesting with medaka (*Oryzias latipes*) suggest that genetic drift unlikely account for the observed differences in life-history traits (64).

Conclusions and implications

Our predictions related to an increase in natural mortality in global fisheries scenarios associated with fisheries-induced evolution of shoaling are based on model simulations and future empirical research is needed to confirm our predictions. Therefore, the direct translation of our findings to real fishing scenarios should be done with great care. The absence of predatory pressure during our experimental evolution removed a selection pressure that could favor the increase in group cohesion despite the presence of size-selective fisheries. Also, the behavioural phenotypes assayed in the present study were measured under controlled conditions in the absence of natural predators. These simplifications should be carefully addressed in future studies. Before such research becomes available and if the simulated scenarios hold in the wild, our results could have implications for global fisheries because selective harvesting of large individuals may affect catchability, recovery and contribute to fisheries-induced evolutionary "suicide" over contemporary time-scales in many shoaling species that happen to form the bulk of global fisheries.

Material and Methods

A. Selection lines. Our study system consisted of wild-collected zebrafish from West Bengal in India (for more details see 38, 65). The parental wild-collected population was experimentally harvested over five generations by exposing them to strong directional selection (a 75 percent per-generation harvest rate) for either small body size (large-harvested line) or large body

DRAFT

size (small-harvested line). A third line was harvested randomly with respect to size and use as a control (random-harvested line). Each selection line was replicated twice for a total of six lines. Size-selective harvesting was applied during the first five generations (6) and then harvesting was stopped for eight further generations until F13 – a time when the present experimental trials took place. At F9 the large-harvested line evolved a smaller adult length and weight and higher relative fecundity compared to controls (6). By contrast, the small-harvested line showed reduced reproductive investment and no change in adult length compared to the control line (6). Both size-selected lines evolved different maturation schedules by maturing smaller and at younger age than the control line (for more details see 6). These differences persisted until F13 as shown elsewhere (31). Overall, the size-selection triggered changes in energy allocation patterns, with the large-harvested line investing early and intensively into reproduction, and the small-harvested line investing early but at low intensity into gonad production and more intensively in somatic growth. Moreover, the selection lines differed significantly in their behavioural traits, size variability, allele frequency and gene expression profiles (6, 31, 35–38)

B. Experimental design. The groups of fish used here are the same of those used to measure collective-risk-taking behavior in a previous study (36), but at different days post fertilization. We stocked 8 juvenile zebrafish at 30 days post fertilization from each of the six selection lines into three-liter rearing boxes. All the boxes were housed on the shelves of the same holding system with a randomized order (6 replicates for each line; N = 12 for each line treatment). Throughout the experiment zebrafish were fed ad libitum with dry food (TetraMin, Tetra), the water temperature was maintained at 26±0.5 °C and photoperiod at 12:12 h light-darkness cycle (light on/off at 07:00 and 19:00, respectively). We run the experimental trials described below when zebrafish were 190 days post fertilization. All trials were run between 09:00 and 14:00. We started the experimental trials two hours after light-on to avoid measuring mating behavior that usually occurs in the first hours after light-on (66). The movement of the fish from the rearing boxes to the experimental tanks was conducted by gently pouring them together with the water from the stocking box. The experimental protocols were approved by the Spanish National Committee and the Committee of the University of Murcia on Ethics and Animal Welfare (CEEA-OH 491/2019).

C. Shoaling experiment. Shoaling behavior in groups of 8 zebrafish was measured in a white round arena (diameter of 60 cm) with 10 cm of water. The arena was placed on a table behind a white curtain to minimize disturbance to the fish during the experimental trials. On top of the arena (at about 1 m) we placed a webcam (resolution: 1920 x 1080 pixels; frame rate: 30 frames per second) that was connected to a computer where video recordings were stored. Zebrafish were introduced in the experimental arena and left undisturbed for 25 min before starting the experimental trial. Video recording lasted 5 min and after that we measured the standard length of each fish on a petri dish with millimeter paper anesthetizing the fish using a clove oil dilution in ethanol and water. The video recordings were analyzed with the idTracker software. The software extracts specific characteristics of each individual and uses them to identify each fish without tagging throughout the video. This method avoids error propagation and is able to fully solve crossing, superposition of animals and occlusion problems (67).

D. Data analysis. We calculated group-level variables for shoaling behavior such as inter-individual distance (i.e., the average distance of a given fish from all the other fish in the arena) and nearest-neighbor distance (i.e., the nearest distance of a given fish from one of the other fish in the arena). We only considered the frames where all the shoal members were detected, and we used the mean body length of the group as a measure of both inter-individual and nearest-neighbor distances (30 out of the 36 trials were used; N = 10 for each line treatment). We also calculated individual-level variables such as speed and burst rate. In this case, the output of the behavioral tracking was filtered by eliminating the coordinates of the individuals with a probability of correct identification lower than 0.85. The conservative filter reduced the number of trials used in the individual analysis (18 out of the 36 trials were used; N = 6 for each line treatment), but it increased the overall quality of the tracking output (on average of more than 90 percent of the fish identities were successfully solved). Our modelling approach focused on burst and coast phases, therefore individual identification was vital because properties of the burst phase, as its duration and rate, can be corrupted by tracking inaccuracy (Fig. S.6). Assuming that the inaccuracy was random, we used a moving average with a Gaussian kernel to correct it. To estimate the standard deviation σ_{smoo} of the Gaussian kernel, we computed the number of burst events in a time interval of 2000 frames and compared it with a manually counted number. The closest approximation of burst events corresponded to $\sigma_{smoo} \approx 1.13$ (Fig. S.7).

E. Statistical approach. Group measurements (inter-individual distance and nearest-neighbor distance) and individual measurements (body size, speed and burst rate) were transformed when necessary by finding the exponent (λ), which made the values of the response variable as normally distributed as possible with a simple power transformation. Then, response variables were modelled using linear mixed effects models with selection lines as fixed effect and selection line replicate as random intercepts. Likelihood ratio tests were used to assess the significant effect of selection lines as fixed effect. Considering that zebrafish behavior is correlated with size (68) and that the size-selective treatments modified the size at age of the selection lines (6), it is conceivable that size differences among the selection lines could have masked evolutionary adaptations in terms of individual behavior. We thus estimated the effect of size (standard length) as a covariate against individual behavior to reveal whether selection treatment per se affected the evolution of behavior, or whether changes in the size of fish indirectly altered behavior in the evolved lines. As regards individual behaviors we implemented a second set of models with the size-matched dataset (Fig. 1D). The response variables were modelled by using linear mixed models and implementing all possible models (i.e., four) with individual body length as covariate, selection lines as fixed effect and selection line replicate as random intercepts. Likelihood ratio tests were used to assess the significant effect of selection lines and body length. All statistical analysis were implemented using R 3.5.0 (https://www.R-project.org/).

F. Shoaling model (burst and coast model). In the agent-based model of shoaling fish, the changes in position and velocity of fish i are described by the following equations of motion:

$$\frac{d\vec{r}_i}{dt} = \vec{v}_i \ , \quad \vec{v}_i = v_i(\cos\varphi_i, \sin\varphi_i)^T \tag{1}$$

$$\frac{dv_i}{dt} = -\beta v_i + \vec{F}_i \cdot \hat{e}_{v,i}, \quad \frac{d\varphi_i}{dt} = \frac{\alpha}{v}\vec{F}_i \cdot \hat{e}_{\varphi,i} \tag{2}$$

with β being the friction coefficient. v_i is the velocity of the focal agent along its heading direction, while φ_i is the polar angle defining the heading direction. $\vec{F}_i \cdot \hat{e}_{v,i}$ and $\vec{F}_i \cdot \hat{e}_{\varphi,i}$ are the projections of the burst force on the heading vector $\hat{e}_{v,i} = (\cos\varphi_i, \sin\varphi_i)$ and the perpendicular direction $\hat{e}_{\varphi,i} = (-\sin\varphi_i, \cos\varphi_i)$, respectively (69).

Fish accelerate only during the burst-phase, which corresponds to a non-zero force $\vec{F}_i$ with magnitude $F = |\vec{F}_i|$ during a burst:

$$\vec{F}_i(t) = F \begin{cases} \hat{f}_{soc}(t) \text{ or } \hat{f}_{env}(t) & \text{during burst} \\ 0 & \text{during coast} \end{cases} \tag{3}$$

This bursting force models the response to either social or environmental cues. During the coast phase no force is applied and fish decelerate due to friction.

Due to the short burst duration ($t_b = 0.12\ s$) the heading may not equal the intended direction (i.e. the force direction). Additionally, experimental data suggests that turning starts prior to the acceleration in velocity direction (Fig. S.6D). Therefore we account for it by introducing a turning parameter $\alpha > 1$ in Eq. 2 that enhances the angular change. For a more detailed motivation and derivation see SI.

The burst behavior is defined by the burst rate γ, duration t_b and the burst force $\vec{F}_i$. The fish decides at the start of a burst with a probability P_{social} to react (socially) to the other fish or, with probability $1 - P_{social}$, to environmental cues. The reaction strength $F = |\vec{F}|$ is for both scenarios the same, only the direction distinguishes them.

The social force direction $\hat{f}_{soc}$ is implemented according to the well established three-zone model (19). A fish reacts to conspecifics by turning away to avoid collisions at short distances $r < r_r$, by aligning at intermediate distances $r_r < r < r_o$, and by being attracted at large distances $r_o < r < r_a$ (Fig. 2A). The direction of the alignment force of fish i is the summation of the velocity differences $\vec{v}_{ji} = \vec{v}_j - \vec{v}_i$ to its nearest neighbors in the alignment zone. We assume interactions with the first shell of nearest neighbors (Voronoi neighbors). Corresponding interaction networks have been shown to approximate well visual interactions (70), and can be very efficiently computed in comparison to visual networks.

DRAFT

If neighbors of the focal fish occupy different zones simultaneously the following rules are applied. If at least one neighbor is in the repulsion zone the alignment and attraction neighbors are ignored. Otherwise, the direction of the social force is a weighted average of the alignment- and attraction-direction. The weights are the number of fish in the respective zone.

If the simulated predator/fishing agent is detected, the environmental force $\hat{f}_{env}$ is given by a direct avoidance force (repulsion) away from it. If no existing threat is detected, the polar angle setting the burst direction due to environmental cues is drawn randomly from a uniform distribution $U(-\Pi, \Pi)$. The latter case is motivated by the fish misinterpreting non-controllable random perturbations (e.g. water reflections) as a threat and responding to them accordingly.

A predator or fishing agent p is detected by fish i with probability

$$P_{i,p,detect} = \frac{2}{1 + r_{pi}/r_f} \tag{4}$$

which equals one if $r_{pi} = |\vec{r}_p - \vec{r}_i| = r_f$. If $P_{detect} > 1$ it is set to 1. r_f is the detection distance which was for all simulations $r_f = 7\ cm$. This value is reasonable because fish should detect a predator with certainty when they are likely to be captured $r_f \geq r_{capture} = 5\ cm$. Note that the detection-probability decays to fifty percent at $r = 21\ cm$.

Additional parameters describing the repulsion force from the wall are avoided by a parameter free wall-avoidance mechanism ensuring that the fish avoids the wall while pursuing its intended direction (see SI for details).

G. Natural predator. The predator always moves directly to the closest simulated fish (Fig. 4A) with $v_{net} = 20,\ 25,\ 30,\ 35\ cm/s$ that larger compared to the speed of the simulated fish ($\langle v \rangle \approx 15\ cm/s$) because predators are usually larger than prey and therefore can swim faster (71, 72). In contrast to a fishing agent, most predators attack a specific fish and therefore need to focus on it before attacking. The so-called confusion effect (73), the disruption of the predator focus by a large number of individuals who are difficult to distinguish by phenotype and movement, is believed to be one key benefit of group living (14). We model the probability of a prey to be successfully captured if it is closer to the predator than $r_{capture} = 5cm$ within a small time window $[t, t + \delta t]$ as

$$p_{success,i}(t, \delta t) = p_{confuse}(t) \cdot \gamma_a \delta t \tag{5}$$

Here $\gamma_a = 1/s$ is a base predator attack rate (representing its handling time) and $p_{confuse}(t)$ represents the confusion effect that modulated the attack rate. The confusion term decreases $p_{success}$ with increasing number of perceived prey (40). A fish is sensed by a predator if it is closer than $r_{sense} = 4r_{capture}$. We assume a sigmoidal dependence on the number of sensed shoaling fish N_{sensed}:

$$p_{confuse} = \frac{\tanh(-(N_{sensed} - N_{conf})) + 1}{2}. \tag{6}$$

Here $N_{conf} = 4$ is the number of sensed shoaling fish at which $p_{confuse} = 0.5$ (73). Thus, each shoaling fish has the same probability to be captured if it is closer to the predator than $r_{capture} = 5\ cm$. Additional parameters needed are summarized in Table S.5.

H. Fishing agents. The fishing agents are assumed to be stationary ($v_{net} = 0\ cm/s$), simulating passive gear or moving at a constant speed $v_{net} = 7.5,\ 15,\ 22.5\ cm/s$, thereby simulating active gear, while shoaling fish move with an average swimming speed ($\langle v \rangle \approx 15\ cm/s$). Fishing agents always capture a shoaling fish if it is closer than $r_{capture} = 5\ cm$. Additional parameters needed for the fishing scenarios are summarized in Table S.5.

H.1. Single fishing agent. In the single fishing agent scenario (Fig. 4A), the agent performs a random search with constant speed v_{net}. For different speed values the angular noise is adapted such that the persistence length is constant. The agent is either stationary (e.g. pots or trap fisheries) or moves randomly (e.g. angler on a boat without information about shoal location) with a fixed persistence length, i.e. its change in angle after travelling a certain distance is independent of its velocity. The angular change is given by

$$d\varphi/dt = \hat{\sigma}_\varphi \xi(t) \tag{7}$$

with $\xi(t)$ as Gaussian white noise. To account for the constant persistence length the noise level is speed dependent $\hat{\sigma}_\varphi = \sigma_\varphi \sqrt{v_{net}}$. See SI for a detailed derivation.

H.2. Multiple fishing agents. In the multiple aligned fishing agents scenario (Fig. 4B), the agents ($N_f = 50$; red) are aligned on a line spanning $L/4$ and they are either stationary (e.g. simulating gill nets or long lines) or moving perpendicular to their linear extension (e.g. simulating a trawling net). After travelling for a distance $L/2$, the fishing agent array is recreated at a distance of $L/4$ away from the center of mass of the shoal and restarts its movement in its direction.

I. Model parameter estimation. The estimated parameters of the model are summarized in Table S.2. The estimation of the friction coefficient β, burst rate γ and duration t_b was done by splitting all data in burst and coast phases. Burst and coast phases were characterized by an increase and decrease in the speed of the shoaling fish, respectively. The friction coefficient β was estimated by the deceleration during coast phases. $\langle t_b \rangle$ was the mean burst length and $\langle \gamma \rangle$ the mean number of a burst events per time unit. However, they are different from the model parameters t_b and γ. Burst events can overlap each other and consequently reduce the measured burst rate and prolong its duration (Fig. S.2B). By a simple binary time series generating model we took account for this effect (See SI Sect. F.1).

The range of the repulsion and attraction zones was difficult to estimate from empirical data, therefore we assumed that the repulsion range r_r corresponded roughly to fish body length (BL) (74, 75), and we estimated $r_r \approx BL/4 \approx 0.5\ cm$ because the ratio of length over width was approximately five. The end of the attraction zone represents, as outer zone, the sensory range of fish for which we assumed $r_a = 30cm$ which corresponds to twelve BL.

J. Model parameter optimization. To fit the model to the empirical data we applied the covariance matrix adaptation evolution strategy (CMA-ES; (76)), from the Python package *pycma* (77). This optimizer is a good choice for multi-modal target functions ("fitness") without known gradients and a high-dimensional search space. We minimized the square-standardized differences between the simulated and experimentally observed values of the nearest-neighbor distances and the average individual speeds which are emergent properties of the model. The differences were standardized by their experimental standard deviation. All parameters were kept equal across the different selection lines apart from the burst rate γ and duration t_b, which were set to fit the experimental values (Fig. S.1), and the tendency to react socially P_{soc}, which was optimized. Next to P_{soc} were the parameters alignment range (r_o), burst force (F) and turning coefficient (α) fitted by the optimizer-algorithm. These four parameters were impossible to be estimated directly from data, however, we could restrict the search space by setting lower and upper bounds (see SI Sect. F, F.1 and Table S.3). The other parameters were set to values estimated in section I. All parameters are summarized in Table S.2.

The optimization result suggested that the vigilance γ_{env} differed among the selection lines as $\gamma_{env}(\text{large-harvested}) > \gamma_{env}(\text{random-harvested}) > \gamma_{env}(\text{small-harvested})$. The generality of this result was substantiated by all different initialization of the optimization(Sect. F.3, Fig. S.9).

K. Data and codes availability. Experimental data are available as supplementary material together with the R code used for statistical analysis. The code to run the burst and coast model, the optimization and the fishing/predator scenarios is fully available upon request.

Bibliography

1. Mikko Heino, Beatriz Díaz Pauli, and Ulf Dieckmann. Fisheries-induced evolution. *Annual Review of Ecology, Evolution and Systematics*, 46(1):461–480, 2015. ISSN 1543-592X. doi: 10.1146/annurev-ecolsys-112414-054339.
2. Fred W. Allendorf and Jeffrey J. Hard. Human-induced evolution caused by unnatural selection through harvest of wild animals. *Proceedings of the National Academy of Sciences, USA*, 106(Supplement 1):9987–9994, 2009. doi: 10.1073/pnas.0901069106.
3. Ken H. Andersen, Lise Marty, and Robert Arlinghaus. Evolution of boldness and life history in response to selective harvesting. *Canadian Journal of Fisheries and Aquatic Sciences*, 75(2):271–281, 2018. ISSN 0706-652X 1205-7533. doi: 10.1139/cjfas-2016-0350.
4. David O. Conover and Stephan B. Munch. Sustaining fisheries yields over evolutionary time scales. *Science*, 297(5578):94–96, 2002. doi: 10.1126/science.1074085.
5. J. Hollins, D. Thambithurai, B. Koeck, A. Crespel, D. M. Bailey, S. J. Cooke, J. Lindstrom, K. J. Parsons, and S. S. Killen. A physiological perspective on fisheries-induced evolution. *Evolutionary Applications*, 11(5):561–576, 2018. ISSN 1752-4571 (Print) 1752-4571 (Linking). doi: 10.1111/eva.12597.

DRAFT

6. Silva Uusi-Heikkilä, Andrew R. Whiteley, Anna Kuparinen, Shuichi Matsumura, Paul A. Venturelli, Christian Wolter, Jon Slate, Craig R. Primmer, Thomas Meinelt, Shaun S. Killen, David Bierbach, Giovanni Polverino, Arne Ludwig, and Robert Arlinghaus. The evolutionary legacy of size-selective harvesting extends from genes to populations. *Evolutionary Applications*, 8(6):597–620, 2015. ISSN 1752-4571. doi: 10.1111/eva.12268.
7. Christian Jørgensen, Katja Enberg, Erin S. Dunlop, Robert Arlinghaus, David S. Boukal, Keith Brander, Bruno Ernande, Anna G. Gårdmark, Fiona Johnston, Shuichi Matsumura, Heidi Pardoe, Kristina Raab, Alexandra Silva, Anssi Vainikka, Ulf Dieckmann, Mikko Heino, and Adriaan D. Rijnsdorp. Ecology: managing evolving fish stocks. *Science*, 318(5854): 1247–1248, 2007.
8. Silva Uusi-Heikkilä, Christian Wolter, Thomas Klefoth, and Robert Arlinghaus. A behavioral perspective on fishing-induced evolution. *Trends in Ecology & Evolution*, 23(8):419–421, 2008. ISSN 0169-5347. doi: 10.1016/j.tree.2008.04.006.
9. FAO. *The state of world fisheries and aquaculture (SOFIA) - meeting the sustainable development goals. Food and Agriculture Organization, Rome, Italy, (p. xiii + 210)*. 2018.
10. Yoo-Won Lee, Tohru Mukai, Kohji Iida, Doo-Jin Hwang, and Hyeong-Il Shin. The application of image processing technology for the analysis of fish school behavior: Evaluation of fish school behavior response to the approaching vessel using scanning sonar. *Fisheries and Aquatic Sciences*, 5(3):212–218, 2002. ISSN 2234-1749.
11. Ole Arve Misund. Avoidance behaviour of herring (*Clupea harengus*) and mackerel (*Scomber scombrus*) in purse seine capture situations. *Fisheries Research*, 16(2):179–194, 1993. ISSN 0165-7836.
12. Maria Tenningen, Gavin J. Macaulay, Guillaume Rieucau, Héctor Peña, and Rolf J. Korneliussen. Behaviours of atlantic herring and mackerel in a purse-seine net, observed using multibeam sonar. *ICES Journal of Marine Science*, 74(1):359–368, 2016. ISSN 1054-3139. doi: 10.1093/icesjms/fsw159.
13. W. D. Hamilton. Geometry for the selfish herd. *Journal of Theoretical Biology*, 31(2):295–311, 1971. ISSN 0022-5193. doi: https://doi.org/10.1016/0022-5193(71)90189-5.
14. Jens Krause and Graeme D Ruxton. *Living in groups*. Oxford University Press, 2002. ISBN 0198508182.
15. TJ Pitcher, AE Magurran, and IJ Winfield. Fish in larger shoals find food faster. *Behavioral Ecology and Sociobiology*, 10(2):149–151, 1982. ISSN 0340-5443.
16. Iain D. Couzin and Jens Krause. *Self-Organization and Collective Behavior in Vertebrates*, volume 32, pages 1–75. Academic Press, 2003. ISBN 0065-3454. doi: https://doi.org/10.1016/S0065-3454(03)01001-5.
17. James E Herbert-Read, Andrea Perna, Richard P Mann, Timothy M Schaerf, David JT Sumpter, and Ashley JW Ward. Inferring the rules of interaction of shoaling fish. *Proceedings of the National Academy of Sciences, USA*, 108(46):18726–18731, 2011. ISSN 0027-8424.
18. Daniel S. Calovi, Alexandra Litchinko, Valentin Lecheval, Ugo Lopez, Alfonso Pérez Escudero, Hugues Chaté, Clément Sire, and Guy Theraulaz. Disentangling and modeling interactions in fish with burst-and-coast swimming reveal distinct alignment and attraction behaviors. *PLOS Computational Biology*, 14(1):e1005933, jan 2018. ISSN 1553-7358. doi: 10.1371/journal.pcbi.1005933.
19. Iain D Couzin, Jens Krause, Richard James, Graeme D Ruxton, and Nigel R Franks. Collective memory and spatial sorting in animal groups. *Journal Theoretical Biology*, 218(1): 1–11, 2002. ISSN 00225193. doi: 10.1006/yjtbi.3065.
20. Robert Arlinghaus, Kate L. Laskowski, Josep Alós, Thomas Klefoth, Christopher T. Monk, Shinnosuke Nakayama, and Arne Schröder. Passive gear-induced timidity syndrome in wild fish populations and its potential ecological and managerial implications. *Fish and Fisheries*, 18(2):360–373, 2017. ISSN 1467-2979. doi: 10.1111/faf.12176.
21. Jolle W. Jolles, Andrew J. King, and Shaun S. Killen. The role of individual heterogeneity in collective animal behaviour. *Trends in Ecology & Evolution*, 2019. ISSN 0169-5347. doi: https://doi.org/10.1016/j.tree.2019.11.001.
22. Zhong-Hua Tang and Shi-Jian Fu. Qingbo (*Spinibarbus sinensis*) personalities and their effect on shoaling behavior. *Acta Ethologica*, 22(2):135–144, 2019. ISSN 0873-9749.
23. Jolle W Jolles, Neeltje J Boogert, Vivek H Sridhar, Iain D Couzin, and Andrea Manica. Consistent individual differences drive collective behavior and group functioning of schooling fish. *Current Biology*, 27(18):2862–2868, 2017. ISSN 0960-9822.
24. Kolbjørn Tunstrøm, Yael Katz, Christos C. Ioannou, Cristián Huepe, Matthew J. Lutz, and Iain D. Couzin. Collective states, multistability and transitional behavior in schooling fish. *PLOS Computational Biology*, 9(2):e1002915, 2013. doi: 10.1371/journal.pcbi.1002915.
25. Ashley J.W. Ward, James E. Herbert-Read, David J.T. Sumpter, and Jens Krause. Fast and accurate decisions through collective vigilance in fish shoals. *Proceedings of the National Academy of Sciences of the United States of America*, 108(6):2312–2315, 2011. ISSN 10916490. doi: 10.1073/pnas.1007102108.
26. Guy Beauchamp. Group-size effects on vigilance: A search for mechanisms. *Behavioural Processes*, 63(3):111–121, 2003. ISSN 03766357. doi: 10.1016/S0376-6357(03)00002-0.
27. Guy Beauchamp. What is the magnitude of the group-size effect on vigilance? *Behavioral Ecology*, 19(6):1361–1368, 2008. ISSN 10452249. doi: 10.1093/beheco/arn096.
28. Sybille Hess, Stefan Fischer, and Barbara Taborsky. Territorial aggression reduces vigilance but increases aggression towards predators in a cooperatively breeding fish. *Animal Behaviour*, 113:229–235, 2016. ISSN 00033472. doi: 10.1016/j.anbehav.2016.01.008.
29. Kenta Uchida, Kei K. Suzuki, Tatsuki Shimamoto, Hisashi Yanagawa, and Itsuro Koizumi. Decreased vigilance or habituation to humans? Mechanisms on increased boldness in urban animals. *Behavioral Ecology*, 30(6):1583–1590, 2019. ISSN 14657279. doi: 10.1093/beheco/arz117.
30. A. M. Edwards, E. C. Best, S. P. Blomberg, and A. W. Goldizen. Individual traits influence vigilance in wild female eastern grey kangaroos. *Australian Journal of Zoology*, 61(4):332–341, 2013. ISSN 0004959X. doi: 10.1071/ZO13025.
31. Valerio Sbragaglia, Josep Alós, Kim Fromm, Christopher T. Monk, Carlos Díaz-Gil, Silva Uusi-Heikkilä, Andrew E. Honsey, Alexander D.M. Wilson, and Robert Arlinghaus. Experimental size-selective harvesting affects behavioral types of a social fish. *Transactions of the American Fisheries Society*, 148(3):552–568, 2019. ISSN 0002-8487 1548-8659. doi: 10.1002/tafs.10160.
32. Richard Bainbridge. The speed of swimming of fish as related to size and to the frequency and amplitude of the tail beat. *Journal of Experimental Biology*, 35(1):109–133, 1958. ISSN 0022-0949.
33. Roy Harpaz, Gašper Tkačik, and Elad Schneidman. Discrete modes of social information processing predict individual behavior of fish in a group. *Proceedings of the National Academy of Sciences, USA*, 114(38):10149–10154, 2017. ISSN 1091-6490 0027-8424. doi: 10.1073/pnas.1703817114.
34. Nikolai W.F. Bode, Jolyon J. Faria, Daniel W. Franks, Jens Krause, and A. Jamie Wood. How perceived threat increases synchronization in collectively moving animal groups. *Proceedings of the Royal Society B: Biological Sciences*, 277(1697):3065–3070, 2010. ISSN 14712970. doi: 10.1098/rspb.2010.0855.
35. V. Sbragaglia, C. Gliese, D. Bierbach, A. E. Honsey, S. Uusi-Heikkila, and R. Arlinghaus. Size-selective harvesting fosters adaptations in mating behaviour and reproductive allocation, affecting sexual selection in fish. *Journal of Animal Ecology*, 88(9):1343–1354, 2019. ISSN 0021-8790. doi: 10.1111/1365-2656.13032.
36. Valerio Sbragaglia, Jose Fernando López-Olmeda, Elena Frigato, Cristiano Bertolucci, and Robert Arlinghaus. Fisheries-induced evolution of the circadian system and collective personality traits. *bioRxiv*, page 622043, 2019. doi: 10.1101/622043.
37. Silva Uusi-Heikkilä, Kai Lindström, Noora Parre, Robert Arlinghaus, Josep Alós, and Anna Kuparinen. Altered trait variability in response to size-selective mortality. *Biology Letters*, 12(9):20160584, 2016. doi: 10.1098/rsbl.2016.0584.
38. S. Uusi-Heikkilä, T. Savilammi, E. Leder, R. Arlinghaus, and C. R. Primmer. Rapid, broad-scale gene expression evolution in experimentally harvested fish populations. *Molecular Ecology*, 26(15):3954–3967, 2017. ISSN 1365-294X (Electronic) 0962-1083 (Linking). doi: 10.1111/mec.14179.
39. Maksym Romenskyy, James E Herbert-Read, Christos C Ioannou, Alex Szorkovszky, Ashley J W Ward, and David J T Sumpter. Quantifying the structure and dynamics of fish shoals under predation threat in three dimensions. *Behavioral Ecology*, 31(2):311–321, 2019. ISSN 1045-2249. doi: 10.1093/beheco/arz197.
40. Manfred Milinski. Experiments on the selection by predators against spatial oddity of their prey. *Zeitschrift für Tierpsychologie*, 43(3):311–325, 1977. ISSN 0044-3573. doi: 10.1111/j.1439-0310.1977.tb00078.x.
41. Josep Alós, Miquel Palmer, and Robert Arlinghaus. Consistent selection towards low activity phenotypes when catchability depends on encounters among human predators and fish. *PLOS ONE*, 7(10):e48030, 2012. doi: 10.1371/journal.pone.0048030.
42. Valerio Sbragaglia, Lorenzo Morroni, Lorenzo Bramanti, Boris Weitzmann, Robert Arlinghaus, and Ernesto Azzurro. Spearfishing modulates flight initiation distance of fishes: the effects of protection, individual size, and bearing a speargun. *ICES Journal of Marine Science*, 75(5):1779–1789, 2018. ISSN 1054-3139 1095-9289. doi: 10.1093/icesjms/fsy059.
43. Katja Enberg, Christian Jørgensen, Erin S. Dunlop, Øystein Varpe, David S. Boukal, Loïc Baulier, Sigrunn Eliassen, and Mikko Heino. Fishing-induced evolution of growth: concepts, mechanisms and the empirical evidence. *Marine Ecology*, 33(1):1–25, 2012. ISSN 1439-0485. doi: 10.1111/j.1439-0485.2011.00460.x.
44. Roy Harpaz and Elad Schneidman. Social interactions drive efficient foraging and income equality in groups of fish. *bioRxiv*, page 740886, 2019. doi: 10.1101/740886.
45. Parisa Rahmani, Fernando Peruani, and Pawel Romanczuk. Flocking in complex environments—attention trade-offs in collective information processing. *PLOS Computational Biology*, 16(4):e1007697, 2020. doi: 10.1371/journal.pcbi.1007697.
46. Pawel Romanczuk, Iain D. Couzin, and Lutz Schimansky-Geier. Collective motion due to individual escape and pursuit response. *Physical Review Letters*, 102(1):010602, jan 2009. ISSN 0031-9007. doi: 10.1103/PhysRevLett.102.010602.
47. Tamás Vicsek, András Czirók, Eshel Ben-Jacob, Inon Cohen, and Ofer Shochet. Novel type of phase transition in a system of self-driven particles. *Physical Review Letters*, 75(6): 1226–1229, aug 1995. ISSN 0031-9007. doi: 10.1103/PhysRevLett.75.1226.
48. Jure Demšar, Charlotte K. Hemelrijk, Hanno Hildenbrandt, and Iztok Lebar Bajec. Simulating predator attacks on schools: Evolving composite tactics. *Ecological Modelling*, 304: 22–33, may 2015. ISSN 03043800. doi: 10.1016/j.ecolmodel.2015.02.018.
49. Randal S. Olson, David B. Knoester, and Christoph Adami. Evolution of swarming behavior is shaped by how predators attack. *Artificial Life*, 22(3):299–318, 2016. doi: 10.1162/ARTL_a_00206%M27139941.
50. Iain D. Couzin, Jens Krause, Nigel R Franks, and Simon A. Levin. Effective leadership and decision making in animal groups on the move. *Nature*, 13(4):513–516, 2005. ISSN 14607425. doi: 10.1038/nature03236.
51. Stephanie M. Carlson, Curry J. Cunningham, and Peter A. H. Westley. Evolutionary rescue in a changing world. *Trends in Ecology & Evolution*, 29(9):521–530, 2014. ISSN 0169-5347. doi: https://doi.org/10.1016/j.tree.2014.06.005.
52. Clémentine Renneville, Alexis Millot, Simon Agostini, David Carmignac, Gersende Maugars, Sylvie Dufour, Arnaud Le Rouzic, and Eric Edeline. Anthropogenic selection along directions of most evolutionary resistance. *bioRxiv*, page 498683, 2018. doi: 10.1101/498683.
53. Serinde J. van Wijk, Martin I. Taylor, Simon Creer, Christine Dreyer, Fernanda M. Rodrigues, Indar W. Ramnarine, Cock van Oosterhout, and Gary R. Carvalho. Experimental harvesting of fish populations drives genetically based shifts in body size and maturation. *Frontiers in Ecology and the Environment*, 11(4):181–187, 2013. ISSN 1540-9309. doi: 10.1890/120229.
54. Katja Enberg, Christian Jørgensen, Erin S. Dunlop, Mikko Heino, and Ulf Dieckmann. Implications of fisheries-induced evolution for stock rebuilding and recovery. *Evolutionary Applications*, 2(3):394–414, 2009. ISSN 1752-4571. doi: 10.1111/j.1752-4571.2009.00077.x.
55. Atle G. Guttormsen, Dadi Kristofersson, and Eric Nævdal. Optimal management of renewable resources with darwinian selection induced by harvesting. *Journal of Environmental Economics and Management*, 56(2):167–179, 2008. ISSN 0095-0696. doi: https://doi.org/10.1016/j.jeem.2007.11.005.
56. Christian Jørgensen and Rebecca E. Holt. Natural mortality: Its ecology, how it shapes fish life histories, and why it may be increased by fishing. *Journal of Sea Research*, 75:8–18, 2013. ISSN 1385-1101. doi: http://dx.doi.org/10.1016/j.seares.2012.04.003.
57. Christian Jørgensen and Oyvind Fiksen. Modelling fishing-induced adaptations and consequences for natural mortality. *Canadian Journal of Fisheries and Aquatic Sciences*, 67(7): 1086–1097, 2010. ISSN 0706-652X. doi: 10.1139/F10-049.
58. Diana M. T. Sharpe and Andrew P. Hendry. Life history change in commercially exploited

fish stocks: an analysis of trends across studies. *Evolutionary Applications*, 2(3):260–275, 2009. ISSN 1752-4571. doi: 10.1111/j.1752-4571.2009.00080.x.

59. Kai Lorenzen. Allometry of natural mortality as a basis for assessing optimal release size in fish-stocking programmes. *Canadian Journal of Fisheries and Aquatic Sciences*, 57(12): 2374–2381, 2000. ISSN 0706-652X. doi: 10.1139/f00-215.
60. Jeffrey A Hutchings. Influence of growth and survival costs of reproduction on atlantic cod, *Gadus morhua*, population growth rate. *Canadian Journal of Fisheries and Aquatic Sciences*, 56(9):1612–1623, 1999. ISSN 0706-652X.
61. Robert NM Ahrens, Carl J Walters, and Villy Christensen. Foraging arena theory. *Fish and fisheries*, 13(1):41–59, 2012. ISSN 1467-2979.
62. David Bierbach, Kate L. Laskowski, and Max Wolf. Behavioural individuality in clonal fish arises despite near-identical rearing conditions. *Nature Communications*, 8:15361, 2017. ISSN 2041-1723. doi: 10.1038/ncomms15361.
63. Nina O Therkildsen, Aryn P Wilder, David O Conover, Stephan B Munch, Hannes Baumann, and Stephen R Palumbi. Contrasting genomic shifts underlie parallel phenotypic evolution in response to fishing. *Science*, 365(6452):487–490, 2019. ISSN 0036-8075.
64. Arnaud Le Rouzic, Clémentine Renneville, Alexis Millot, Simon Agostini, David Carmignac, and Éric Édeline. Unidirectional response to bidirectional selection on body size ii quantitative genetics. *bioRxiv*, page 2020.01.23.916361, 2020. doi: 10.1101/2020.01.23.916361.
65. S. Uusi-Heikkilä, C. Wolter, T. Meinelt, and R. Arlinghaus. Size-dependent reproductive success of wild zebrafish *Danio rerio* in the laboratory. *Journal of Fish Biology*, 77(3):552–69, 2010. ISSN 0022-1112. doi: 10.1111/j.1095-8649.2010.02698.x.
66. K. O. Darrow and W. A. Harris. Characterization and development of courtship in zebrafish, *Danio rerio*. *Zebrafish*, 1(1):40–5, 2004. ISSN 1545-8547. doi: 10.1089/154585404774101662.
67. Alfonso Pérez-Escudero, Julián Vicente-Page, Robert C. Hinz, Sara Arganda, and Gonzalo G. de Polavieja. idtracker: tracking individuals in a group by automatic identification of unmarked animals. *Nature Methods*, 11(7):743–748, 2014. doi: 10.1038/nmeth.2994https://www.nature.com/articles/nmeth.2994#supplementary-information.
68. G. Polverino, D. Bierbach, S. S. Killen, S. Uusi-Heikkila, and R. Arlinghaus. Body length rather than routine metabolic rate and body condition correlates with activity and risk-taking in juvenile zebrafish *Danio rerio*. *Journal of Fish Biology*, 89(5):2251–2267, 2016. ISSN 0022-1112. doi: 10.1111/jfb.13100.
69. Pawel Romanczuk, Markus Bär, Werner Ebeling, Benjamin Lindner, and Lutz Schimansky-Geier. Active brownian particles. *The European Physical Journal Special Topics*, 202(1): 1–162, 2012.
70. Ariana Strandburg-Peshkin, Colin R. Twomey, Nikolai W F Bode, Albert B. Kao, Yael Katz, Christos C. Ioannou, Sara B. Rosenthal, Colin J. Torney, Hai Shan Wu, Simon A. Levin, and Iain D. Couzin. Visual sensory networks and effective information transfer in animal groups. *Current Biology*, 23(17):R709–R711, 2013. ISSN 09609822. doi: 10.1016/j.cub.2013.07.059.
71. Paolo Domenici. The scaling of locomotor performance in predator–prey encounters: from fish to killer whales. *Comparative Biochemistry and Physiology Part A: Molecular & Integrative Physiology*, 131(1):169–182, 2001. ISSN 1095-6433. doi: https://doi.org/10.1016/S1095-6433(01)00465-2.
72. Howard C Howland. Optimal strategies for predator avoidance: the relative importance of speed and manoeuvrability. *Journal of Theoretical Biology*, 47(2):333–350, 1974. ISSN 0022-5193.
73. Laurie Landeau and John Terborgh. Oddity and the 'confusion effect'in predation. *Animal Behaviour*, 34(5):1372–1380, 1986. ISSN 0003-3472.
74. Yael Katz, Kolbjørn Tunstrøm, Christos C. Ioannou, Cristián Huepe, and Iain D. Couzin. Inferring the structure and dynamics of interactions in schooling fish. *Proc. Natl. Acad. Sci. U. S. A.*, 108(46):18720–18725, 2011. ISSN 00278424. doi: 10.1073/pnas.1107583108.
75. Maud I. A. Kent, Ryan Lukeman, Joseph T. Lizier, and Ashley J. W. Ward. Speed-mediated properties of schooling. *R. Soc. Open Sci.*, 6(2):181482, feb 2019. ISSN 2054-5703. doi: 10.1098/rsos.181482.
76. Nikolaus Hansen and Andreas Ostermeier. Adapting arbitrary normal mutation distributions in evolution strategies: The covariance matrix adaptation. *Proceedings of IEEE International Conference on Evolutionary Computation*, pages 312–317, 1996. doi: 10.1109/ICEC.1996.542381.
77. Nikolaus Hansen, Youhei Akimoto, and Petr Baudis. Cma-es/pycma on github. Zenodo, DOI:10.5281/zenodo.2559634, 2019.

DRAFT

Supporting Informations

Supplementary Note 1: Model description

The burst-coast model intends to mimic the burst-coast swimming behavior of zebrafish (*Danio Rerio*). We assume that a fish is accelerating only during the burst phase with a constant force of magnitude f_b, while no forces are present during the coast phase implying a deceleration due to friction. The differential equations of motion defining current position $\vec{r}_i$ and velocity $\vec{v}_i$ of an agent i are:

$$\frac{d\vec{r}_i}{dt} = \vec{v}_i \tag{S.1a}$$

$$\frac{d\vec{v}_i}{dt} = -\beta\vec{v}_i + \vec{F}_i(t) \tag{S.1b}$$

with $\vec{F}_i(t)$ as a finite social or environmental force vector with $|F(t)| > 0$, for fish in the bursting phase. A fish decelerates passively during the coasting phase, thus the force vector vanishes $|\vec{F}_i| = 0$. β is the friction coefficient. We consider the social or environmental force vector to determine the preferred heading direction of the fish following a burst phase. Since the burst duration was very short (see section I), the resulting heading direction of the shoaling fish might diverge from the direction of the force. After a visual check of the experimental video material, we observed the characteristic zigzag-like swimming of zebrafish. This was also evident in the trajectories of the fish (Fig. S.6) and the corresponding force parallel and perpendicular to the current velocity. The turning force often started prior to the acceleration in velocity direction and reached its maximum at the start of the burst. To account for this we split the velocity change of Eq.(S.1) into the part parallel and perpendicular to the current velocity direction $\vec{v} = v[cos(\varphi), sin(\varphi)]$ and introduce a turning parameter $\alpha > 1$ which enhance the angular change:

$$\frac{d\vec{v}}{dt} = \frac{dv}{dt}\vec{e}_r + v\vec{e}_\varphi\frac{d\varphi}{dt} \tag{S.2a}$$

$$\frac{dv_i}{dt} = -\beta v_i + \vec{F}_i \cdot \hat{e}_r \tag{S.2b}$$

$$\frac{d\varphi_i}{dt} = \frac{\alpha}{v}\vec{F}_i \cdot \hat{e}_\varphi. \tag{S.2c}$$

Note that for a point-like particle responding to an external force α must be exactly 1. The above extension was required to account in our dynamical equations of motion for the fast active turning of zebrafish prior to acceleration along the direction of motion observed in our tracking data. Furthermore, note that the v^{-1} dependence of the angular change was, next to being directly derived from Eq. (S.1), verified by the tracking data (Fig. S.4).

The burst behavior is defined by the burst rate γ, the burst time or duration of the burst t_b, and the burst force $\vec{F}$. In particular the burst force $\vec{F}$ governs whether the fish uses social or environmental cues. The fish decides at the start of a burst with a probability P_{social} if reacting socially to the other fish or, with probability $1 - P_{social}$, to environmental cues.

The resulting burst force $\vec{F}$ is

$$\vec{F} = \begin{cases} F\hat{f}_{soc}, & \text{if } p < P_{soc} \text{ with } p \sim U(0,1) \\ F\hat{f}_{env}, & \text{otherwise} \end{cases} \tag{S.3}$$

with F as the magnitude of the burst force and $\hat{f}_{env}$, $\hat{f}_{soc}$ as the unit vectors in direction of the environmental or social cue.

A. Social forces. The social force is motivated by a three zone model (19) consisting of a repulsion zone ending at a distance r_r, followed by the alignment zone ending at r_o, and the attraction zone ending at r_a. Thereby it is $r_r < r_o < r_a$. The direction of the social forces is computed by

$$\hat{f}_{i,rep} = \mathcal{N}\left(\sum_{j\in\mathbb{S}_{i,r}} -\hat{r}_{ji}\right) \tag{S.4a}$$

$$\hat{f}_{i,alg} = \mathcal{N}\left(\sum_{j\in\mathbb{S}_{i,o}} \vec{v}_{ji}\right) \tag{S.4b}$$

$$\hat{f}_{i,att} = \mathcal{N}\left(\sum_{j\in\mathbb{S}_{i,a}} \hat{r}_{ji}\right) \tag{S.4c}$$

DRAFT

with $\hat{x} = \vec{x}/|x|$ defining a unit vector, $\vec{x}_{ji} = \vec{x}_j - \vec{x}_i$ as the difference between the vectors of fish j and i, $\mathbb{S}_{i,x}$ is the set of indices of fish in zone x of fish i, and $\mathcal{N}(\vec{x}) = \hat{x}$ is a normalization operator. We assume Voronoi interactions because they provide a reasonable approximation to visual networks (70) and can be efficiently computed. Therefore the sets $\mathbb{S}_{i,x}$ with $x \in [r, o, a]$ are composed only of Voronoi neighbors of fish i. Note that the alignment force is the sum of the velocity difference vectors $\vec{v}_{ji}$. Thus the focal fish i experiences the strongest alignment with neighbours whose velocity vectors differed the most from its own.

If neighbors of fish i are occupying different zones simultaneously the following rules are applied:

- if $\mathbb{S}_r \neq \emptyset$: $\hat{f}_{soc} = \hat{f}_r$ (repulsion dominated)
- if $\mathbb{S}_r = \emptyset$ and $\mathbb{S}_o \neq \emptyset$ and $\mathbb{S}_a \neq \emptyset$: $\hat{f}_{soc} = \mathcal{N}(|\mathbb{S}_a|\hat{f}_a + |\mathbb{S}_o|\hat{f}_o)$ (weighted average)

B. Environmental force. In the absence of a predator the environmental force is modelled as a random force vector. This models the sensitivity of individual fish to environmental noise (e.g. water reflections, water perturbations, sounds), and to a resulting false-positive escape response. In the presence of a threatening agent the environmental force is modelled as a simple repulsion of the shoaling fish from the simulated predator or fishing agents

$$\hat{f}_{env} = \begin{cases} [cos(\varphi), sin(\varphi)] \text{ with } \varphi \sim U(-\Pi, \Pi) & \text{no predator present, } \mathbb{S}_{i,p} = \emptyset \\ \mathcal{N}\left(\sum_{p \in \mathbb{S}_{i,p}} -\hat{r}_{pi}\right) & \text{otherwise} \end{cases} \tag{S.5}$$

with $U(a,b)$ being a uniform distribution with a and b as lower and upper bounds, and $\mathbb{S}_{i,p}$ being the set of predator or fishing agents detected by a shoaling fish i. A predator or fishing agent is detected by a shoaling fish with probability $P_{detect} = \frac{2}{1+r_{pi}/r_f}$ which equals one at $r_{pi} = r_f$. If $P_{detect} > 1$ it is set to 1. r_f is the detection distance which was for all simulations $r_f = 7\ cm$. This value is reasonable because fish should be able to detect a predator when they are likely to be captured $r_f \geq r_{capture} = 5\ cm$ but the distance should also be close to $r_{capture}$, otherwise fish would respond too often to non-dangerous cues and because the visibility in water decays with distance. The randomness is a consequence of the assumption that shoaling fish misinterpret reflections on the water surface as threats since there were no "real" threats in the experiment.

C. Wall-avoidance mechanism. We attempt to design the model as close to the experimental setting as possible and therefore use a circle as a boundary. The introduction of parameters describing the repulsion force from the wall was avoided by the fish following a parameter free wall-avoidance mechanism. It is based on predicting before each burst the future position $\vec{r}_{fut}$ of the shoaling fish at the next expected burst. If $\vec{r}_{fut}$ is outside of the tank, at the next burst, we compute the position at which the shoaling fish would collide with the wall. The overall force is adapted such that at the end of the coast the velocity of the shoaling fish aligns parallel to the wall. This ensures that the shoaling fish avoids the wall while pursuing its intended direction.

D. Capture probability of a single fish by a natural predator. If a shoaling fish is closer to the predator than $r_{capture}$ its probability to be successfully captured within a small time window $[t, t+\delta t]$ is

$$p_{success}(t, \delta t) = p_{confuse}(t) \cdot \gamma_a \delta t. \tag{S.6}$$

Here γ_a is the predator attack rate, and $p_{confuse}(t)$ represents the confusion effect that modulates the attack rate. The attack rate used in the simulations is $\gamma_a = 1/s$. The confusion term depends on the spatial configuration of shoaling fish around the predator and decreases $p_{success}$ the more individuals are sensed (40). A shoaling fish is sensed if it is closer than $r_{sense} = 4 \cdot r_{capture}$. We assume that it modulates the successful capture probability in a sigmoidal way depending on the number of sensed shoaling fish N_{sensed}:

$$p_{confuse} = \frac{\tanh(-(N_{sensed} - N_{conf})) + 1}{2}. \tag{S.7}$$

Here $N_{conf} = 4$ is the number of sensed shoaling fish at which $p_{confuse} = 0.5$.

E. Random movement of angling agent with constant persistence length. The individual fishing agent is supposed to have a constant persistence length. It's angular change is given by

$$\frac{d\varphi}{dt} = \hat{\sigma}_\varphi \xi(t). \tag{S.8}$$

$\xi(t) \propto \mathbb{N}(0,1)$ is Gaussian white noise with zero mean and variance of one. $\hat{\sigma} = \hat{\sigma}(v_{net})$ is the angular noise strength whose exact form and dependence is derived below.

DRAFT

Keeping the persistence length constant is equivalent with keeping the variance in angle constant after the individual fishing agent travelled a path of length = l. The time needed to travel this path-length is $t_l = l/v_f$ and the variance in angle after travelling the path is

$$Var(\varphi)(l, v_{net}) = \langle \varphi(l, v_{net})^2 \rangle \tag{S.9a}$$

$$= \langle \left(\int_0^{t_l} \hat{\sigma}_\varphi \xi(t) dt \right)^2 \rangle = \hat{\sigma}_\varphi^2 \int_0^{t_l} \int_0^{t_l} \langle \xi(t)\xi(t') \rangle dt dt' \tag{S.9b}$$

$$= \hat{\sigma}_\varphi^2 \int_0^{t_l} \int_0^{t_l} \delta_{t,t'} dt dt' = \hat{\sigma}_\varphi^2 \int_0^{t_l} dt \tag{S.9c}$$

$$= \hat{\sigma}_\varphi^2 t_l = \hat{\sigma}_\varphi^2 \frac{l}{v_{net}}. \tag{S.9d}$$

Here we used that the Gaussian white noise is uncorrelated, e.g. $\langle \xi(t)\xi(t') \rangle = \delta_{t,t'}$, with $\delta_{t,t'}$ as the Kronecker-delta. If we set $\hat{\sigma}_\varphi = \sigma_\varphi \cdot \sqrt{v_{net}}$, the variance in angle after travelling a path of length l is independent of the speed:

$$Var(\varphi)(l) = \hat{\sigma}_\varphi^2 \frac{l}{v_{net}} \tag{S.10a}$$

$$= \sigma_\varphi^2 \cdot l. \tag{S.10b}$$

F. Parameter setting. The model has in total nine parameter, from which three can be estimated from experimental measures. The remaining six parameter which can not be directly accessed from data were either (i) set by simple heuristics (2 parameters) or (ii) indirectly estimated by an optimization (4 parameter). The optimization minimized the sum of squared differences between model emergent properties and their experimental measured values. For a full overview of all model-parameters and how they are set see Figure S.2A. First, section F.1 explains the parameter estimation from experimental measures in detail. Second, section F.2 names the heuristic for setting the attraction and repulsion range. Last, section F.3 explains the optimization of the remaining parameters. All model parameters are summarized in Table S.2.

F.1. Parameter estimation from experimental data. Since in the model (see section F) an agent can be either in the burst or coast phase we split individual trajectories in these phases. Burst and coast phases are characterized by an increase and decrease in the speed of the shoaling fish, respectively. In the coast phase the only parameter which defines change in velocity is the friction coefficient β (Eq. S.2). Thus we estimated $\beta = 2.51$ by the slope of the linear regression between the response in speed to the current speed of the fish during coast-phases as seen in Figure S.5. Because the friction force is by definition zero at zero velocity we fixed the interception point to zero and therefore found effectively the least-square solution of the linear equation $\frac{dv}{dt} = -bv$.

The average burst duration $\langle t_b \rangle$ and rate $\langle \gamma \rangle$ were estimated by the mean length and frequency of burst periods. For the large-, random- and small-harvested line the burst duration was $\langle t_b \rangle = [0.117, 0.123, 0.123]s$ and the burst rate was $\langle \gamma \rangle = [0.35, 0.44, 0.38]$ respectively. In the model a new burst period can start during an already ongoing burst and therefore prolong the measured burst duration and decrease the rate as illustrated in Figure S.2B. Consequently is the average burst duration and rate different from the model-parameters t_b and γ. We approximated them by creating a binary time series in which at each time-step dt a burst-event happens with probability $\gamma * dt$ which raises the acceleration from zero to F for a duration of t_b. We simulated this process, computed the average values $\rangle t_b \langle_N$, $\rangle \gamma \langle_N$ (as seen in Figure S.2B) and selected the γ and t_b which minimized the summed square differences to the experimental observed averages for each harvested line. In Figure S.1 the squared differences are shown. The resulting parameters are reported in Table S.2.

The burst force F in heading direction $f_{b,s}$ can be estimated by adding to the change in speed $\frac{dv}{dt}$ the friction coefficient times the current velocity $\beta \cdot v$ as illustrated in Figure S.2C. This results in the mean burst force in heading direction $f_{b,s} = 95cm/s^2$. However, from Eq. S.2 it is clear that the total magnitude of the burst force is defined as

$$f_b = \sqrt{f_{b,s}^2 + f_{b,\varphi}^2} \tag{S.11}$$

with $f_{b,\varphi} = \frac{d\varphi}{dt} \cdot v$ (from Eq. S.2c with $\alpha = 1$). Note, that we are using f_b instead of the symbol for the model parameter F because in the above equation we neglect the impact of the turning parameter α by setting it to one. We estimated the mean $\langle f_b \rangle = 132.6cm/s^2$ and standard-deviation $\sigma_{f_b} = 31.1cm/s^2$. Instead of setting $F = f_b$ we were using its mean and standard-deviation to set the boundaries of the search-space for F in the optimizer. This is reasonable because we can not estimate α from the data and in consequence can not be certain about the value of F needed to reproduce the bursting behavior experimentally observed.

DRAFT

F.2. Parameter setting by heuristics. For the parameters attraction r_a and repulsion range r_r the estimation from data is difficult. Since the attraction range limits the outer zone of the three-zone model it represents the sensory range. By setting $r_a = 30$ we assume a sensory range of about twelve body lengths.

A rough estimate for the repulsion range is possible from the pair density profile as computed in (74, 75) for different fish species. In these studies the density shows a sudden increase at a side-distance between 0.25 and one body lengths. We used in this study $r_r \approx BL/4 \approx 0.5cm$. Note that the range can be below one BL because the ratio of length over width is for the zebrafish around five.

F.3. Parameter optimization by covariance matrix adaptation evolution strategy. To fit the model to the data we applied the CMA-ES (76, 77). This optimizer is a good choice if the fitness landscape is multi-modal, the search space dimension is between 5 and 100 and no gradient is known. The optimizer minimizes the error function

$$E(\mathbb{P}_{LH}, \mathbb{P}_{RH}, \mathbb{P}_{SH}) = \frac{Err(\mathbb{P}_{LH}) + Err(\mathbb{P}_{RH}) + Err(\mathbb{P}_{SH})}{3} \tag{S.12}$$

with $\mathbb{P}_{\text{SL}}$ as the set of parameter of a selection line (SL) needed to run a simulation. Therefore it is the mean of the errors of the individual selection lines which compare simulation with exprimental measures. The error of a specific selection lines compares the measured nearest neighbour distance NND and average individual speed v to the experimental data by computing the sum of the squared differences standardized by their experimental standard deviation:

$$Err(\mathbb{P}_{\text{SL}}) = \left(\frac{\langle \text{NND} \rangle_{exp,\text{SL}} - \langle \text{NND} \rangle_{sim,\text{SL}}}{\sigma_{nnd}} \right)^2 + \left(\frac{(\langle \text{v} \rangle_{exp,\text{SL}} - \langle \text{v} \rangle_{sim,\text{SL}}}{\sigma_v} \right)^2 . \tag{S.13}$$

Here $(\langle \text{x} \rangle_{exp,\text{SL}}$ and $(\langle \text{x} \rangle_{sim,\text{SL}}$ are the experimentally and simulation based measured values for x for a specific selection line and σ_x is the corresponding experimental standard deviation. The for the error function used experimental measures for NND and v for the specific selection lines are listed in Table S.3.

At each generation the parameter sets are updated by the CMA-ES. Note that the parameter sets differ only in burst duration, rate, and probability to respond to social cues in between the selection lines. From these three parameters only the probability to follow social cues P_{soc} is modified by the algorithm. Consequently the search-space is 6-dimensional (r_o, F, α, $P_{soc,LH}$, $P_{soc,RH}$, $P_{soc,SH}$) as highlighted in Table S.2.

We limited the search-space of the algorithm for the four different parameters by setting boundaries which are listed in Table S.3. The lower and upper boundary for the alignment range were the repulsion and attraction range respectively. For the probability to follow social cues we ensured a minimum attention to social and environmental cues by setting the boundaries 0.05 above and below the theoretical possible boundaries of zero and 1. The boundaries of the burst force F are two standard deviation below and above the mean burst force computed from experimental data by assuming $\alpha = 1$, as explained in section F.1. The turning parameters lower boundary is one while the upper one was set to 15 assuming a sufficient enhanced turning ability at this setting.

To ensure that the resulting minimum is not a local minimum we repeated the optimization from different initial parameter settings. The initial parameter were selected from a four-dimensional grid with 2 grid-points and therefore $2^4 = 16$ different initial parameter settings. Note that the actual search-space is 6-dimensional and by setting P_{soc} for the different selection line initially equal we reduce the number of initial settings from $2^6 = 64$ to 16.

An example optimization run over 400 generations is shown in Figure S.8. The optimization outcomes of the 16 different initialization are shown sorted by their final error according to Eq. S.12 in Figure S.9. The unexpected results - that the nearest-neighbor distance is larger for the less risk-taking large-harvested line - can be explained by assuming that the risk-taking is reflected in the model parameter to follow environmental cues. Therefore the following inequality is expected: p_{soc} (large-harvested line: LH) < p_{soc} (random-harvested line: RH) < p_{soc} (small-harvested line: SH). Only for the optimization with the largest error this inequality is violated which is marked in Figure S.9G by a blue background. This ensures the generality of the inequality.

Supplementary Note 2: Mean distance of shoaling fish to fishing agents

Here we computed the mean distance the shoaling fish kept from fishing agents. This measure is an alternative to the exploitation rate used in the main text, to quantify how well the shoaling fish avoid capture:

$$\langle d_{if} \rangle = \frac{1}{N} \sum_{i=1}^{N} \min_{f \in \mathbb{S}_f} d_{if} \tag{S.1}$$

with $d_{if} = |\vec{r}_{if}|$ as the distance between shoaling fish i and a fishing agent f. The minimum function yields the distance to the closest fishing agent. In Figure S.3I, J, K, L show the relative and M, N, O, P the normal mean distance to the predator.

DRAFT

The distance measured substantiated the already reported results for the exploitation rate. Note that in the natural-predator scenario (I, M) the differences between selection lines is qualitatively equivalent to the other scenarios in contrast to the scenario comparison with the exploitation rate(A, E). This is reasonable because the confusion effect, the main difference between the natural predator and the other fishing agents, affects the ability of the predator to catch prey and not the ability of the prey to avoid the predator.

Movie-S1.avi. This movie shows simulations in the circular area with parameters adjusted such that only the wall avoidance mechanism changes the path of the shoaling fish. The parameters are the ones estimated for the random harvested line listed in Table S.2 apart for the repulsion, alignment and attraction range and probability to follow social cues P_{soc}. Those parameters were set such that the agents always responded to social information $P_{soc} = 1$, but never had any neighbors due to short ranges $r_r = r_o = r_a = 0.001cm$. Thus the agents effectively swim always straight until they come in conflict with the wall. Then the wall avoidance mechanism started.

Movie-S2.avi. Eight shoaling fish are simulated in a circular area with fitted social interaction. The parameters were the ones estimated for the random harvested line listed in Table S.2.

Movie-S3.avi. Thirty agents simulated in a rectangle of length $L = 100cm$ with periodic boundary conditions in the predator scenario. The parameters were the ones estimated for the random harvested line listed in Table S.2 and additional fishing/predator scenario parameters listed in Table S.5. Note that the predator, in red, moves with a speed of $v_p = 20cm/s$ and therefore faster as the average velocity of shoaling fish. However, it moves directly to the closest prey and therefore covers the prey until it get killed. Due to the confusion effect the killing probability was lowered and it happens that the predator stays for a notable time above the targeted fish.

Movie-S4.avi. Thirty agents simulated in a rectangle of length $L = 100cm$ with periodic boundary conditions in the angler scenario. The parameters were the ones estimated for the random harvested line listed in Table S.2 and additional fishing/predator scenario parameters listed in Table S.5.

Movie-S5.avi. Thirty agents simulated in a rectangle of length $L = 100cm$ with periodic boundary conditions in the trawling scenario. The parameters were the ones estimated for the random harvested line listed in Table S.2 and additional fishing/predator scenario parameters listed in Table S.5.

DRAFT

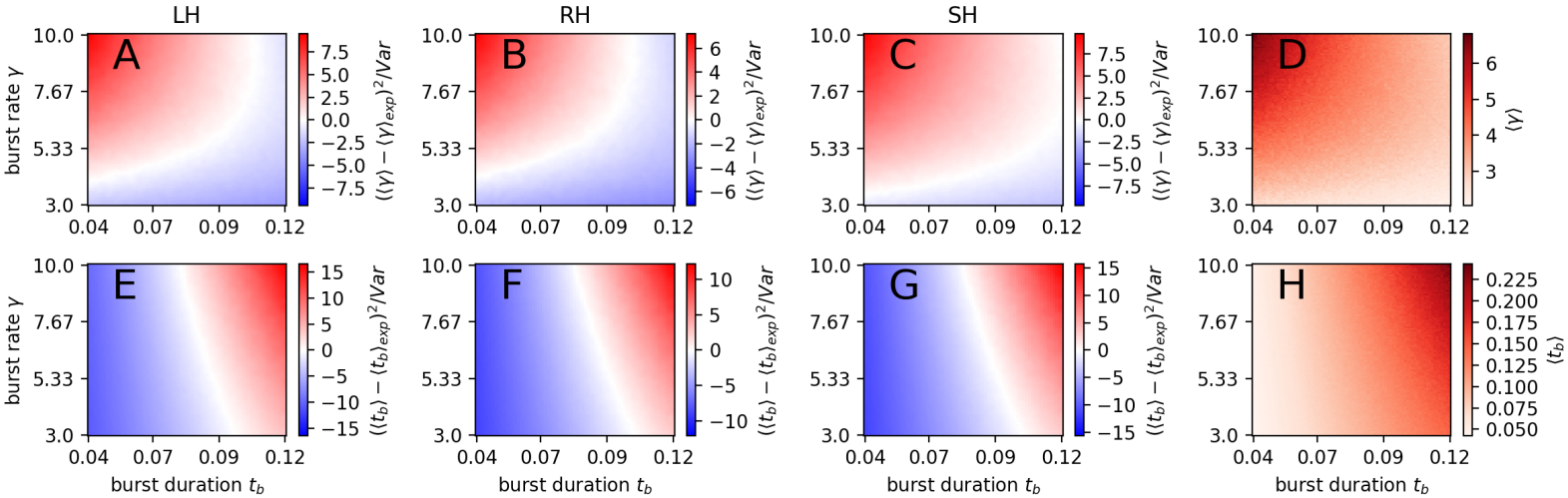

Fig. S.1. Model parameter estimation of burst duration t_b and burst rate γ (parameters of an acceleration-time-series generating model). The acceleration-based-average is reported for burst rate $\langle\gamma\rangle$ (**A-D**) and burst duration (**E-H**) $\langle t_b\rangle$. The normalized squared difference between the averaged values of the simulation $\langle x\rangle$ and the experiment $\langle x\rangle_{exp}$ are shown for large-harvested line (LH; **A, E**, random-harvested line (RH; **B, F**) and small-harvested line (SH;**C, G**). The average values of the simulation are shown in (**D, H**). Note that **A, B, C** are **D** minus the experimental mean burst rate of the respective selection line. Same for **E, F, G** which are **H** minus the exp. mean burst duration.

DRAFT

Scenario	Speed	Distribution	Lines	Estimate	P/z value
natural predator	20	Gaussian	LH	0.0017	<0.001
			SH	0.0001	0.344
	25	Gaussian	LH	0.0021	<0.001
			SH	-0.0002	0.103
	30	Gaussian	LH	0.0020	<0.001
			SH	-0.0005	<0.001
	35	Gaussian	LH	0.0023	<0.001
			SH	-0.0007	<0.001
single fishing agent	0	Quasipoisson	LH	-1.982	<0.001
			SH	0.3240	<0.001
	7.5	Quasipoisson	LH	-1.191	<0.001
			SH	0.399	<0.001
	15	Gaussian	LH	-0.0011	<0.001
			SH	0.0013	<0.001
	22.5	Gaussian	LH	-0.0006	<0.001
			SH	0.0008	<0.001
multiple fishing agents	0	Quasipoisson	LH	-0.9773	<0.001
			SH	0.3059	<0.001
	7.5	Gaussian	LH	-0.0255	<0.001
			SH	0.0164	<0.001
	15	Gaussian	LH	-0.0901	<0.001
			SH	0.1694	<0.001
	22.5	Gaussian	LH	-0.0596	<0.001
			SH	0.1786	<0.001

Table S.1. Statistical modeling of relative exploitation rate for the three different scenarios (predator, single fishing agent, and multiple fishing agents). Estimates are shown together with the P/z values and the distribution used to model the response variable for each speed of the predator/fishing agent at which the simulations have been run. Estimates for the large-harvested line (LH) and small-harvested line (SH) are shown with respect to the control line that was randomly selected for size.

model parameter	symbol	estimated value	estimation method	unit
repulsion range	r_r	$\langle BL \rangle /4 \approx 0.5$	heuristics	cm
attraction range	r_a	30	heuristics	cm
alignment range	r_o	16.2	optimizer	cm
burst force	F	93.4	optimizer	cm/s^2
turning parameter	α	14.8	optimizer	1
prob. of social burst	P_{soc}	LH: 0.66 RH: 0.81 SH: 0.83	optimizer	1
burst duration	t_b	LH: 0.089 RH: 0.091 SH: 0.097	data+model	s
burst rate	γ	LH: 5.7 RH: 6.3 SH: 4.7	data+model	$1/s$
friction coefficient	β	2.51	data	$1/s$

Table S.2. Model parameters of the burst-coast model and their estimates. The estimation methods are colored according to the colors used in Figure S.2A. For the parameters P_{soc}, t_b and γ each selection line has its specific value which is marked by the abbreviations LH: large-harvested; RH: random-harvested and SH: small-harvested.

DRAFT

optimization parameter	symbol	optimization boundaries	unit
alignment range	r_o	$[0.5, 30]$ $(=[r_{rep}, r_{att}])$	cm
burst force	F	$[70.4,\ 194.8]$ $(=[\langle f_b\rangle - 2\sigma_{f_b},\ \langle f_b\rangle + 2\sigma_{f_b}])$	cm/s^2
turning parameter	α	$[0,\ 15]$	1
prob. of social burst	P_{soc}	$[0.05,\ 0.95]$	1
error function defining measures	**symbol**	**experimental mean and STD**	**unit**
individual speed	v	LH: 15 ± 2.8 RH: 17 ± 2.5 SH: 13.2 ± 2.7	cm/s
nearest neighbor dist.	NND	LH: 6.4 ± 1 RH: 5.8 ± 1.1 SH: 5.6 ± 0.9	cm

Table S.3. The first part of the table shows the upper and lower boundaries in which the optimizer searched for the minimum of the error function Eq. S.12. The lower and upper boundary of the burst force F are given by the mean minus and plus twice the standard deviation of the experimental estimated burst force$\langle f_b\rangle$ respectively. The second part of the table lists the measures defining the error function Eq. S.12, which is minimized by the optimizer.

Line	Replicate	Symbol in Fig.2A	NND	IID
LH + SH	1+2	circles	$\chi^2_{(2)} = 8.8;\ p < 0.05$	$\chi^2_{(2)} = 7.8; p < 0.05$
LH	1	triangles	$\chi^2_{(2)} = 15.8;\ p < 0.001$	$\chi^2_{(2)} = 19.0;\ p < 0.001$
LH	2	crosses	$\chi^2_{(2)} = 0.6;\ p = 0.739$	$\chi^2_{(2)} = 4.8;\ p = 0.090$
SH	1	triangles	$\chi^2_{(2)} = 4.08;\ p = 0.129$	$\chi^2_{(2)} = 3.1;\ p = 0.212$
SH	2	crosses	$\chi^2_{(2)} = 7.2;\ p < 0.05$	$\chi^2_{(2)} = 7.8;\ p < 0.05$

Table S.4. Results of the statistical modelling assessing the effect of selection lines on nearest-neighbor distance (NND) and inter-individual distance (IID). Results presented in the main text accounted for both replicates of each of selection line as random effects (LH + SH). Next the replicates (1 and 2) of each selection lines (LH and SH) have been kept one at a time to assess consistent results at the statistical level.

scenario related parameter	symbol	value	scenario relevance	unit
flee range[a]	r_f	7	all	cm
fishers/predators capture range	$r_{capture}$	5	all	cm
predators sensing range	r_{sense}	$4r_{capture} = 20$	natural pred.	cm
confusion number	N_{conf}	4	natural pred.	cm
attack rate	γ_a	1	natural pred.	$1/s$
angular noise strength	σ_φ	0.2	single fisher	$1/s^{1/2}$

Table S.5. Parameters used to simulate interaction of fish with predator/fisher in different scenarios. The column "scenario relevance" specifies for which scenario the parameter is needed. [a]: Note that the flee range influences the probability of a prey detecting a predator/fisher (Eq. 4) which is 0.5 at a distance of $21cm$ given $r_f = 7cm$. Therefore the range of the prey to detect a predator is comparable to the predators sensing range.

DRAFT

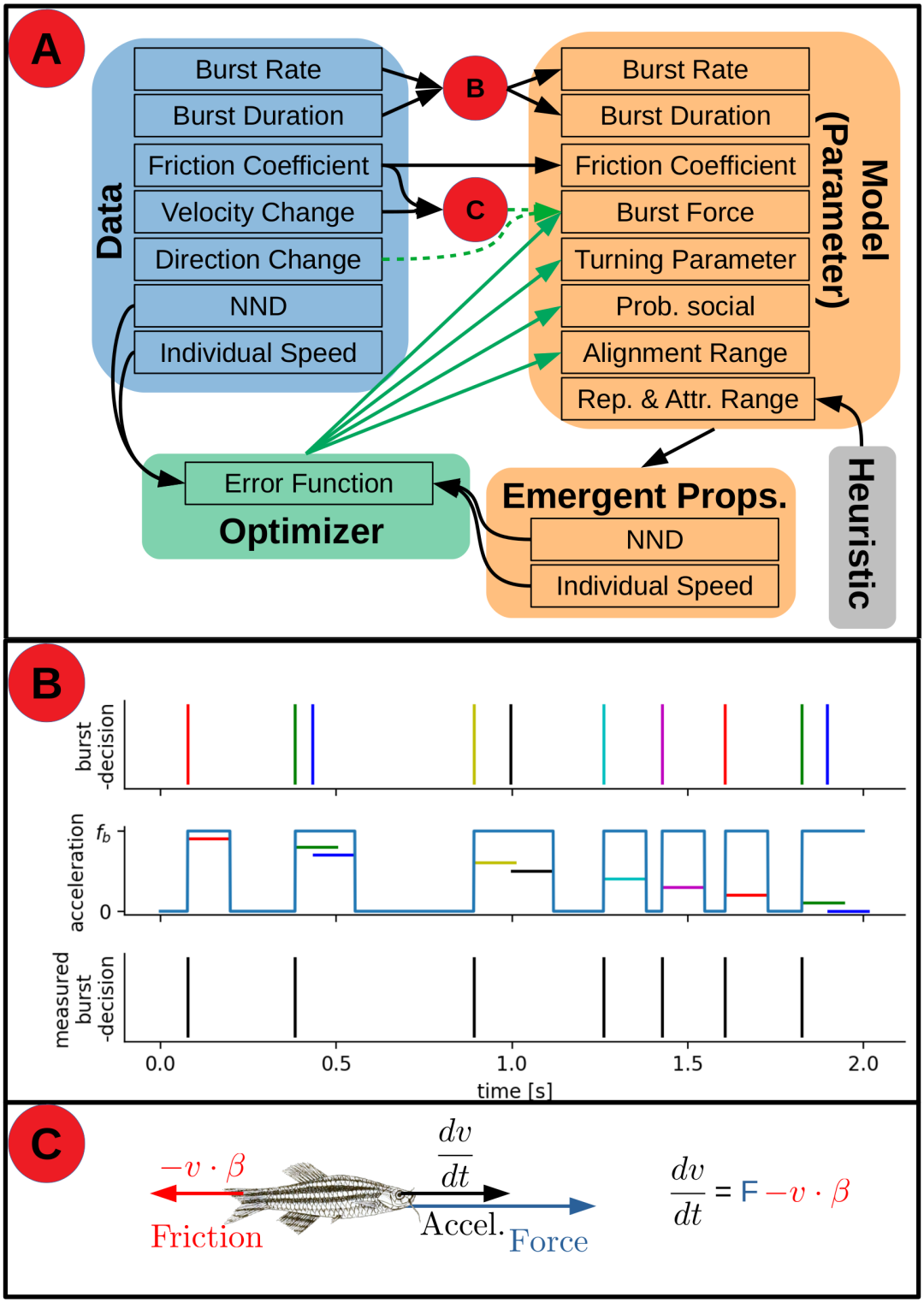

Fig. S.2. Sketched relations between the experimental measures, optimizer results and the model-parameters (**A**). Illustration of how the burst-decision (based on the model-parameter burst rate γ) links via the acceleration and burst-duration (t_b) to the measured burst-decision and therefore the measured burst rate $\langle\gamma\rangle$ and duration $\langle t_b\rangle$ (**B**). Sketched relation between the force F the fish needs to cause a change in speed $\frac{dv}{dt}$ and the friction defined by the friction coefficient β (**C**).

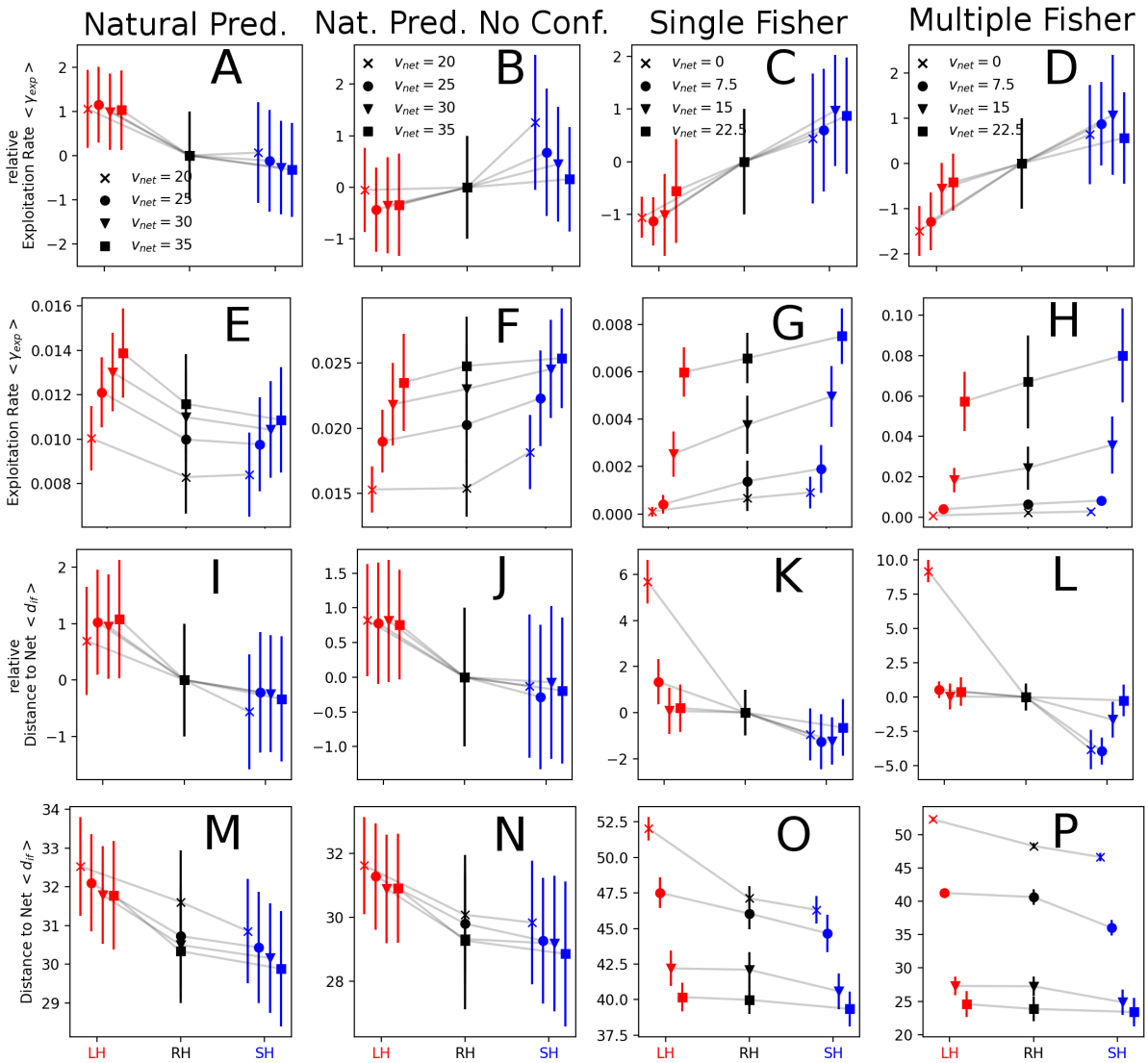

Fig. S.3. Mean values of different measures are shown for the (**A, E, I, M**) "natural predator", (**B, F, J, N**) "natural predator without confusion", (**C, G, K, O**) "single fishing agent" and (**D, H, L, P**) "multiple fishing agent" scenario. $N = 30$ shoaling fish were simulated in a box of size $L = 100\ cm$ with periodic boundary conditions. Their mean individual speed was about $\langle v \rangle \approx 15\ cm/s$. The predator moved with $v_{net} = [20,\ 25,\ 30,\ 35]\ cm/s$ while the fishing agents with $v_{net} = [0,\ 7.5,\ 15,\ 22.5]\ cm/s$ indicated by star, circle, triangle and square marker, respectively. The first and second row show the relative and normal mean exploitation rate γ_{exp} respectively. The third and forth row are the relative and normal mean distance to the predator/fishing agent d_{if} respectively. The relative measures were computed by reducing the non-relative measures by the mean and dividing them by the standard deviation of the random-harvested line. The symbols and error bars represent the mean and standard deviation computed from samples of 400 simulations. Note that the pattern in exploitation rate γ_{exp} for the natural predator (**A, E**) is the inverse pattern of the other scenarios (**B, C, D, F, G, H**). However, for the distance to predator/fishing agent d_{if} the pattern $LH(d_{if}) > RH(d_{if}) > SH(d_{if})$ is found in all scenarios because the confusion only impacts the probability of the predator to successfully catch a prey, not the ability of prey to avoid the predator.

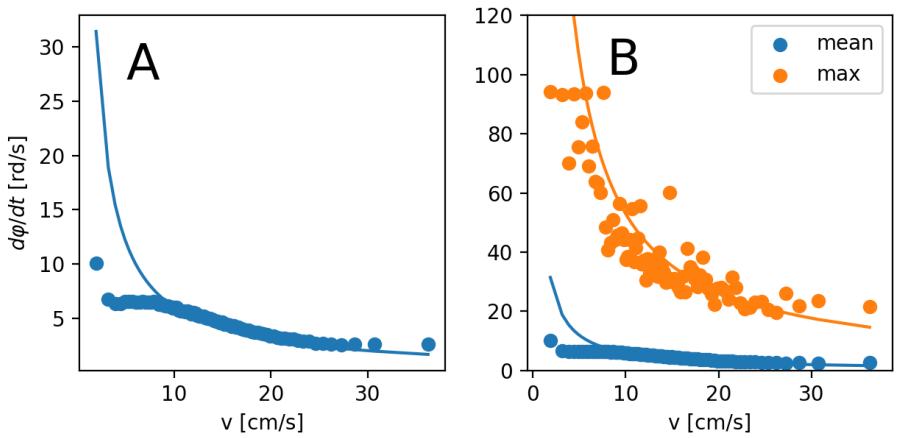

Fig. S.4. Angular change $d\varphi/dt$ depending on the velocity v. The blue dots (**A, B**) represent the mean values while orange dots (**B**) the maximum observed value for the binned data. The lines are not fitted to the data but serve as an comparison to inverse proportionality. The blue line is $f(v) = 6/v$ and the orange line is $f(v) = 530/v$. The resemblance of the data to the lines supports the model assumption in Eq. (S.2c).

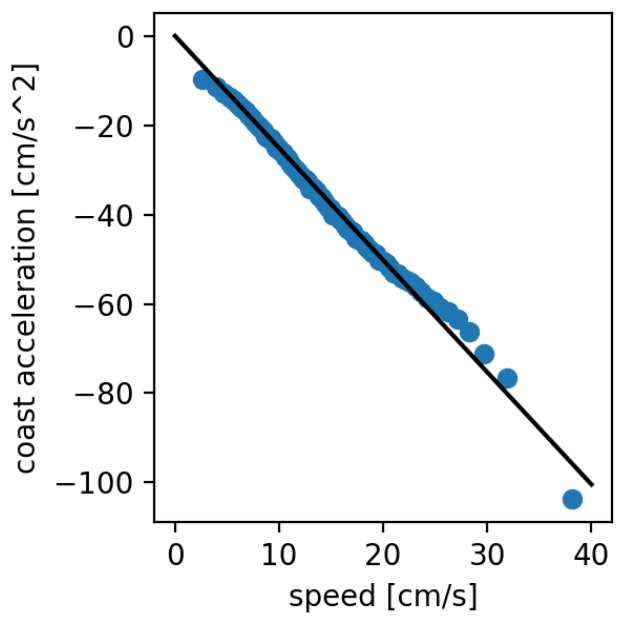

Fig. S.5. Estimation of friction coefficient from experimental data. Dots represent mean of bins with varying width such that each bin contains an equal amount of data. Black line shows linear fit with the interception at zero and the negative friction coefficient as slope $-\beta = -2.51$.

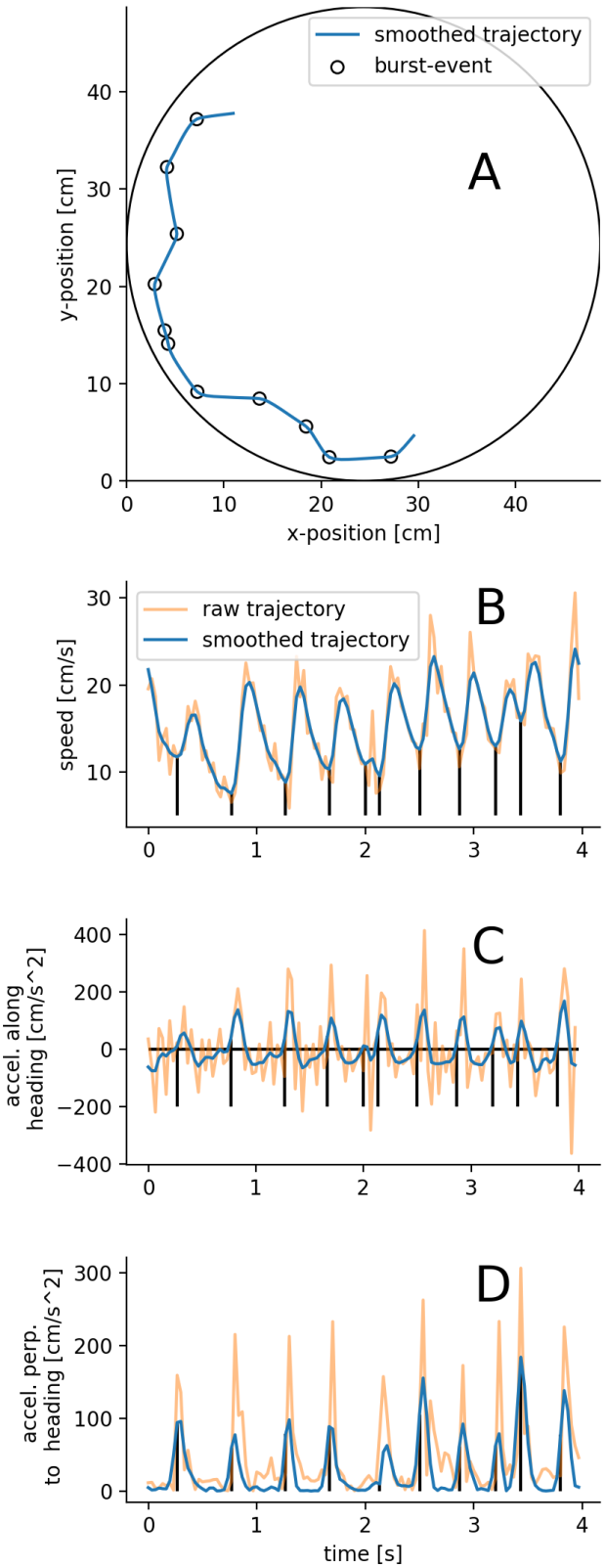

Fig. S.6. Example smoothed trajectory of a swimming zebrafish generated from ID-Tracker data (**A**). The large circle represents tank-boundary. For this trajectory the speed (**B**), acceleration along (**C**) and perpendicular (**D**) to heading direction are shown computed from the raw (orange) and smoothed (blue) trajectory. The black circles (**A**) and vertical black lines (**B, C, D**) indicate burst events which are are the onsets of a positive acceleration period of the smoothed data (**C**).

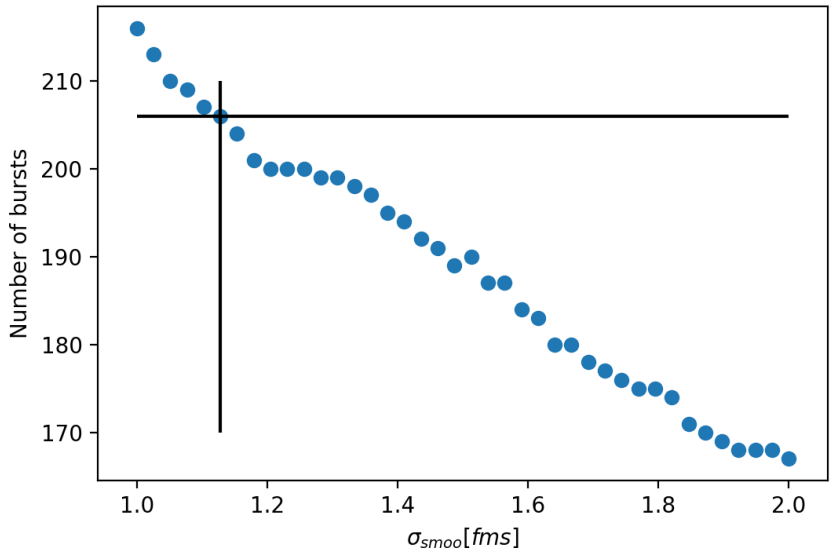

Fig. S.7. Number of burst events of a randomly selected trajectory spanning 2000 frames. The horizontal black line marks the number of manually counted burst events. Blue dots mark automatic counts of burst events on a smoothed trajectory using a moving window with a Gaussian kernel of varying standard deviation σ_{smoo}. The vertical black line indicates the standard deviation $\sigma_{smoo} = 1.13 fms$ where the automatic burst detection equals the manually counted one.

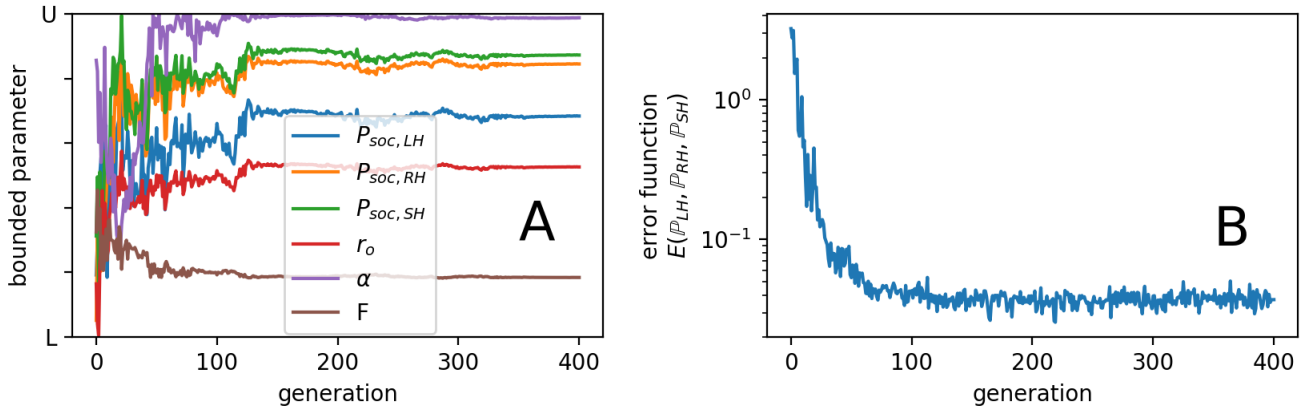

Fig. S.8. Example of optimization run with the parameters giving the lowest error in the current generation (**A**) and the corresponding error (**B**). The parameters are normalized according to their respective lower and upper boundary (see Table S.3) which are marked on the y-axis with L and U (**A**). Different colors mark the probability to respond to social cues P_{soc} of the large (blue), random (orange) and small harvested line (green), the alignment range r_o (red), turning parameter α (violet) and the burst force F (brown).

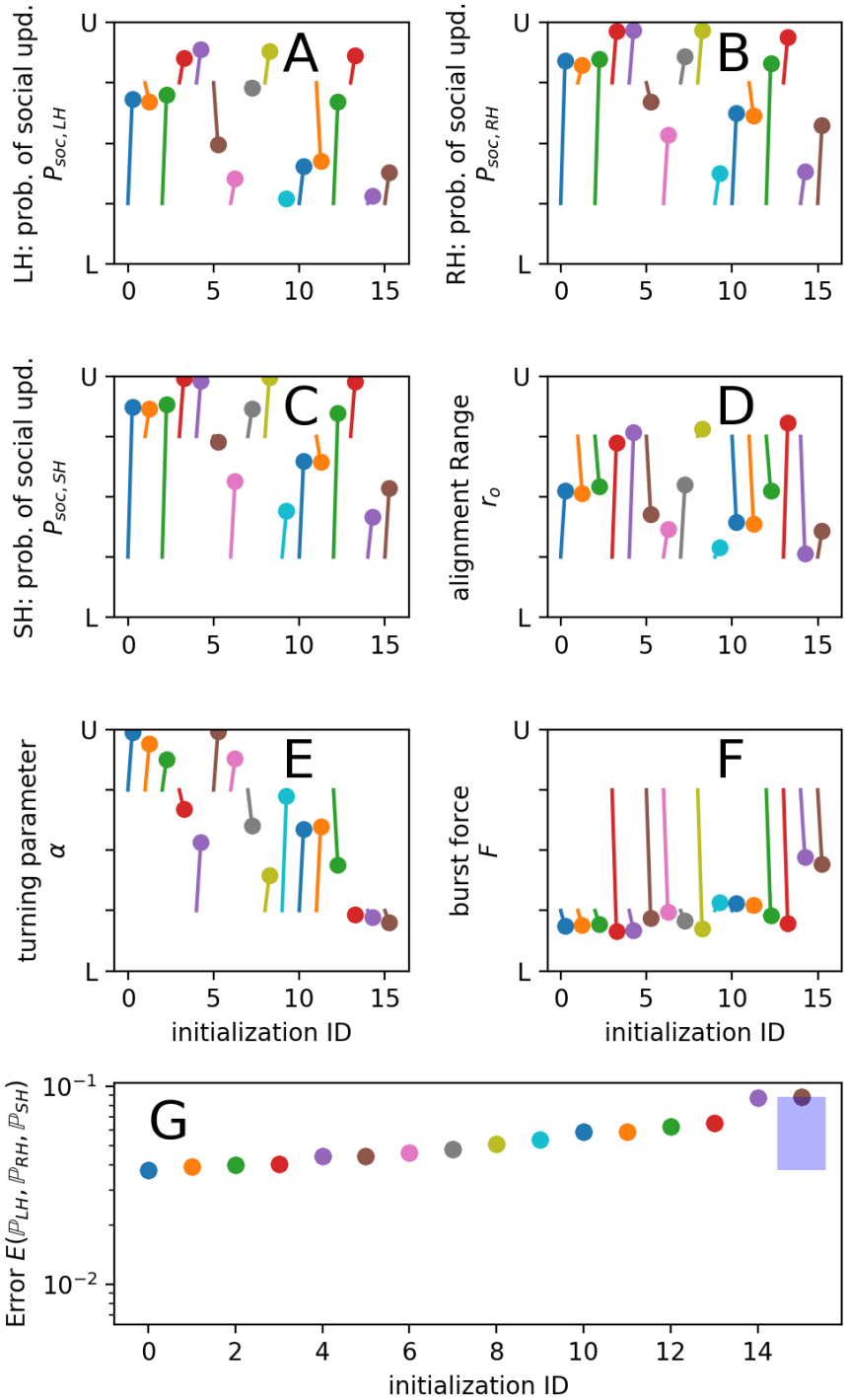

Fig. S.9. Initial and final parameters (**A-F**) together with final error (**G**) according to Eq. S.12 for the 16 different initialized optimization runs. The initialization are sorted such that the one with the best outcome, i.e. with the smallest error, is first. Colors mark specific initialization ID and are consistent across subfigures. The circles (**A-F**) mark the final parameter while the other end of the line marks the initial setting. The light blue and red background-color (**G**) marks an outcome different to $P_{env,LH} > P_{env,RH} > P_{env,SH}$ and $\gamma_{env,LH} > \gamma_{env,RH} > \gamma_{env,SH}$. Note that the former inequality does not enforce the latter since each selection line has a different burst-rate γ which influences the environmental burst rate as $\gamma_{env} = P_{env}\gamma$.